A direct interareal feedback-to-feedforward circuit in primate visual cortex

Caitlin Siu
University of Utah
Justin Balsor
University of Utah
Frederick Federer
University of Utah
Alessandra Angelucci (alessandra.angelucci@hsc.utah.edu)
University of Utah https://orcid.org/0000-0002-1957-2231

Article

Keywords: Mammalian Sensory Neocortex, Hierarchical Computation, FF-FB Loops,

Posted Date: September 2nd, 2020

DOI: https://doi.org/10.21203/rs.3.rs-50399/v1

Version of Record: A version of this preprint was published at Nature Communications on August 13th, 2021. See the published version at https://doi.org/10.1038/s41467-021-24928-6.

Submitted to: Nature Neuroscience

A direct interareal feedback-to-feedforward circuit in primate visual cortex

Caitlin Siu[1], Justin Balsor[1], Frederick Federer[1], and Alessandra Angelucci[1,*]

[1] Department of Ophthalmology and Visual Science, Moran Eye Institute, University of Utah, 65 Mario Capecchi Drive, Salt Lake City, UT 84132, USA.

* Correspondence to: alessandra.angelucci@hsc.utah.edu

ABSTRACT

The mammalian sensory neocortex consists of hierarchically organized areas reciprocally connected via feedforward (FF) and feedback (FB) circuits. Several theories of hierarchical computation ascribe the bulk of the computational work of the cortex to looped FF-FB circuits between pairs of cortical areas. However, whether such corticocortical loops exist remains unclear. In higher mammals, FF projections send afferents almost exclusively to a single higher-level area. However, it is unclear whether FB projections show similar area-specificity, and whether they influence FF-projection neurons directly or indirectly. Using viral-mediated monosynaptic circuit tracing in macaque visual cortex, we find that neurons sending FF projections to a higher-level area receive monosynaptic FB inputs exclusively from that area. We also find monosynaptic FB-to-FB neuron contacts as a second motif of FB connectivity. Our results support the existence of FF-FB loops in primate cortex, and suggest that FB can rapidly and selectively influence the activity of incoming FF signals.

INTRODUCTION

In the neocortex, sensory information is processed within hierarchically-organized areas reciprocally connected via feedforward (FF) and feedback (FB) circuits [1,2]. FF connections carry information from lower to higher-level areas. As information ascends through the cortical hierarchy, neuronal receptive fields (RFs) become tuned to increasingly complex stimulus features, and an increasingly abstract representation of sensory inputs is achieved. FF connections are reciprocated by FB connections sending information from higher to lower areas. This hierarchy is further organized into parallel processing streams, so that cortical areas within each stream are functionally specialized to process specific attributes of a sensory stimulus [3,4]. Reciprocal FF-FB connections between pairs of cortical areas are found throughout the neocortex of all mammalian species, suggesting they play a fundamental computation, but their role remains poorly understood.

Traditional feedforward models of sensory processing postulate that FF connections mediate the complexification of RFs, and that object recognition occurs largely independently of FB signals [5-7], the latter purely serving strategic processing and attentional selection. In contrast, several theories of hierarchical computation postulate that most of the computational work of the cortex is carried out by information going back and forth over looped FF-FB circuits between pairs of interconnected areas [8-16]. The exact computation performed by these loops depends on the specific theory, but many of these theories require FF-FB loops to occur between neurons in different areas processing similar stimulus attributes, albeit at different levels of abstraction. Whether this anatomical organization of FF-FB loops indeed exists in the cortex remains unclear. It is well established that most cortical areas possess reciprocal FF and FB connections [17,18]. However, since each area projects to, and receives inputs from, multiple areas, it is less clear whether FF and FB connections selectively contact the neurons that are the source of their reciprocal areal input, or rather unselectively contact different projection neurons in their target area. It is also unclear whether these cortico-cortical loops occur via direct monosynaptic contacts between FF and FB projection neurons, or indirectly via local excitatory or inhibitory neurons, or both. Recent studies have shown that in mouse primary visual cortex (V1), only a fraction of cortical projection neurons form area-specific monosynaptic FF-FB loops [19], and that these loops may only occur between deep layer neurons [20]. It remains unknown whether similar rules of cortico-cortical connectivity apply to higher mammals.

In cats and primates, inter-areal FF projections are highly area-specific, much more so than in rodents. For example, only a small percent of FF-projecting V1 neurons send a common input to multiple extrastriate areas via bifurcating axons [21-23]. However, it is less clear whether FB projections show similar area specificity, and whether they influence FF projection neurons directly or indirectly. On the one hand, previous reports that neurons in extrastriate cortex sending FB projections to V1 and the secondary visual area (V2) contain substantial amounts of axonal bifurcations [21,24-26] and form diffuse terminations [27-29] suggest that FB may not selectively contact the neurons that are the source of their areal input. On the other hand, recent demonstrations of clustered and specific FB terminations in primate V1 [30] (see also [31]) suggest the opposite.

To address this question, here we adapted viral-mediated monosynaptic input tracing methods [32] to label the inputs to V1 neurons sending FF projections to V2 in macaque visual cortex. We find that V1 cells projecting to V2 receive monosynaptic inputs from V2 FB neurons, but not from neurons in other extrastriate areas known to also send FB projections to V1. Thus, in primates FB connections send area-specific inputs to the cells that are the source of their areal input. We

also find evidence for direct corticocortical FB-to-FB contacts. These results suggest that FB can rapidly and highly selectively influence the activity of incoming FF signals, and support the existence of area-specific FF-FB loops in the primate early visual cortex.

RESULTS

Monosynaptic Input Tracing in Macaque Cortex

Figure 1 about here

We adapted viral-mediated monosynaptic input tracing or TRIO (TRacing Inputs and Outputs [32,33]) to identify, in macaque visual cortex, direct presynaptic inputs to V1 neurons projecting to V2 (V1→V2 neurons). We used an intersectional viral strategy based on three different viral vectors injected at different times (**Fig. 1a**; see Methods). We injected in V1 a mixture of two Cre-dependent adeno-associated viruses serotype 9 (AAV9), one carrying the gene for the avian tumor virus receptor A (TVA receptor for EnvA) fused with the red fluorescent protein mCherry (AAV9-CAG-FLEX-TVAmCherry), the other carrying the gene for the optimized rabies virus glycoprotein (oG [34]) (AAV9-CAG-FLEX-oG-WPRE). After about 3 weeks, necessary for the AAV genome to concatermerize, a canine adenovirus type 2 carrying Cre-recombinase (CAV2-CMV-Cre [33,35]) was injected in V2 at retinotopic locations matched to those of the V1 injections. CAV2 is a retrograde vector that rapidly transcribes Cre-recombinase in local V2 neurons and V1→V2 neurons projecting to the CAV2 injection site in V2, reaching maximum expression in 5-7 days. In the presence of Cre, in V1 only the V1→V2 cells previously infected with AAV9-FLEX vectors express mCherry (thus, turning red; **Fig.1a,c,d**), TVA and oG. About one week after the CAV2 injections, EnvA-pseudotyped, G-deleted rabies virus (RV*dG*) carrying the gene for green fluorescent protein (eGFP) (EnvA-RV*dG*-eGFP) was injected in V1 at the same location as the AAV9 injections. Since the EnvA ligand binds exclusively to the TVA receptor, which is not otherwise native in the primate brain, RV*dG* can only infect cells that express TVA. This results in the expression of GFP in TVA-expressing V1→V2 cells, which become double labeled in red and green (yellow "starter" cells in **Fig. 1a,c,d**). Moreover, the presence of oG in the starter cells, allows RV*dG* complementation and retrograde monosynaptic spread of the rabies virus, with consequent GFP expression in the presynaptic input cells, which turn green (**Fig.1a,c,d**). As the input cells do not express oG, RVdG cannot further spread trans-synaptically beyond these neurons. To ensure retinotopic overlap of the injections in V2 and V1, we used *in vivo* intrinsic signal optical imaging (OI) as guidance, and made 2-3 injections of the AAV9 and 2-3 injections of the RV*dG* vectors in V1, and 1-2 injections of CAV2-Cre in V2 as shown in **Figure 1b** (see Methods). The V1 injections spanned all cortical layers, while the V2 injections were centered in layer (L)4, where the bulk of V1 FF projections terminate. The V1 and V2 injection sites for an example case are shown in **Figs. 1c, 2a-b** and **3a-b, 4a-b** respectively.

The above protocol resulted in GFP labeling of both intra-V1 and extra-V1 monosynaptic inputs to the V1→V2 starter cells. Control experiments (n=2) further demonstrated that all of the inputs arising from outside V1, and the vast majority of the intra-V1 inputs arising from beyond

400 μm from the injection site were dependent on CAV2-Cre, and that non-specific infection of RV*dG* only occurred nearby the location of the injection site **(Extended Data Fig. 1**). It has been well-documented in mouse models that this non-specific local label is caused by small amounts of TVA "leak" [32,33]. Because in our control experiments 75% of all non-specific GFP label was located within 355 μm of the injection site center, in our quantitative analyses we omitted any GFP labeled cells within a 400μm radius of the injection site.

V1→V2 Neurons Receive Monosynaptic Inputs from V2 FB Neurons

Here we present results from TRIO experiments performed in 3 macaque monkeys to label monosynaptic inputs to V1→V2 neurons.

V1 Starter Cells

Figure 2 about here

We first determined the laminar distribution of starter (double-labeled) cells in V1 resulting from the TRIO protocol described above. **Figures 1b-d and 2a-d** show the V1 injection sites and resulting labeled neurons in V1 for one example case (MK405) in which starter cells were observed in all V1 layers known to send projections to V2 (layers 2/3, 4A, 4B, 5, 6), albeit the vast majority (~90%) of starter cells were located in L2/3. In cases MK382 and MK379, starter cells were located in all V2-projecting layers except L6, and while more abundant (~80%) in the superficial layers (i.e. above L4C), a significant fraction (~20%) was located in L5. The majority of superficial layer cells were located in L2/3 in case MK379, while they were more evenly distributed across superficial layers in case MK382. Consistent with the well-documented lack of V1→V2 projection neurons in L1 and 4C, we found no labeled starter cells in these layers in any of the cases (**Fig. 2e**), supporting the cell specificity of our viral approach. Across the 3 cases, on average 62.2±16.5% of V1→V2 starter cells were located in L2/3, and 85% were located in the superficial layers (**Fig. 2f**). The larger percent of V1 starter cells in the superficial layers is consistent with the laminar origin of V1-to-V2 projections which arise predominantly (96-98%) from the superficial layers[36,37]. We measured the distance of each starter cell from the nearest V1 injection site center for each case (**Fig. 2g**; see Methods). Across the population of starter cells, 75% of cells were located within 538.3±126.7 μm of the nearest injection site center (average mean distance± s.e.m.: 392.4±98.12 μm; average median±s.e.m.: 369.9±98.76 μm). The spatial distribution of starter cells in V1 reflects the spatial spread and overlap of the injected viruses. The retinotopic overlap of the V2 and V1 injections was also confirmed by the presence of mCherry-labeled axon terminals in layers 4 and lower 3 of V2 within about 1 mm of the V2 injection site (**Fig. 3a-b**).

V2 Starter Cells

Figure 3 about here

In two cases (MK405, MK379), we found a few double-labeled cells in V2 **(Fig. 3a-c**). Expression of mCherry in V2 neurons could only occur if the latter were co-infected retrogradely by both the CAV2 and AAV9 vectors, indicating these cells sent intra-areal lateral connections to the CAV2

injection site in V2 as well as FB projections to any of the AAV9 injection sites in V1; therefore, these are V1 projecting V2 FB cells (V2→V1). This is possible as retrograde transfection of neurons by AAV9 vectors, although less efficient than anterograde infection, is known to occur [38]. Expression of GFP in these mCherry-expressing V2 cells could have resulted from retrograde infection of their TVA-expressing terminals in V1 by the rabies vector, known to occur [39], or from trans-synaptic spread of the rabies virus from V1 starter cells. In the latter scenario, these double labeled V2 neurons would represent FB cells sending monosynaptic inputs to V1→V2 starter cells as well as intra-areal projections to the V2 injected site. However, our approach does not allow us to distinguish between these two possibilities. In principle, these double-labeled V2 cells could represent a potential confound in our study, as any GFP-labeled neurons throughout the brain could be presynaptic to these V2→V1 "starter" cells and/or to the V1→V2 starter cells whose inputs we intended to trace. However, we believe this potential confound is minimal, as in only one case, MK379, did the V2 starter cells represent a more substantial fraction (17%, n=11 cells) of the total number of starter cells. In the other two cases, instead, V2 starter cells were either absent (MK382) or represented a tiny fraction (2%, n=12 cells) of the total number of starter cells (MK405); therefore, it is safe to assume that all or most of the input cells, respectively, in the latter two cases are presynaptic to the V1→V2 starter neurons. **Figure 3d** shows the laminar distribution of the V2 starter cells. In case MK405 75% (n=9) of V2 starter cells were located in L2/3 and 25% (n=3 cells) in L5, while in case MK379 all V2 starter cells (n=11) were located in L5. Consistent with our interpretation that the V2 starter cells send FB connections to the V1 injection sites, we observed no double-labeled cells in V2 layers that are not the source of FB projections, i.e. L1 and 4. V2 starter cells were located at a distance of up to 2 mm from the injection site (average mean distance± s.e.m.: 845±174.35 μm; average median±s.e.m.:758±194.1 μm; **Fig. 3e**), on average about twice the distance of V1 starter cells from the nearest V1 injection site (**Fig.2g**). This supports the interpretation that the CAV2 vector infected these cells at their terminals within V2, and indicates these neurons send long-range horizontal connections within V2, in addition to providing FB to V1.

Monosynaptic V2 FB Inputs to V1→V2 Starter Cells

Figure 4 about here

In all 3 cases we found GFP-labeled input cells in V2, in both the superficial and deep layers (**Fig. 4**). It is well known that the superficial and deep layers of V2 are the source of FB inputs to V1, but our results show that at least some of these FB inputs make direct monosynaptic contacts with V1→V2 neurons. In the superficial layers, input cells were located throughout L2/3, but appeared more numerous in L3 (**Fig. 4a**). However, because, the border between V2 L2 and L3 is not easily identifiable in the tangential sectioning plane, we did not attempt to distinguish between these two layers. In the deep layers, input cells were located in both L5 and 6, but were much more numerous in L5 (**Fig. 4b-c**). In the two cases that had either no (MK382) or a very small percentage of (MK405) starter cells inV2, the V2 input cells arose in almost similar amounts from superficial and deep layers (**Fig. 4c**); these FB cells make monosynaptic contacts with V1→V2 starter cells. Only 3 cells were found in L4 in case MK405, and, since L4 does not project out of V2, these cells are likely presynaptic to the few V2 starter cells found in this case. In contrast to these two cases, in case MK379, which had a larger fraction of V2 starter cells, we found a much larger percentage

of V2 input cells in L5 (74.7%, n=896 cells) (**Fig. 4c**). As all V2 starter cells in this case were located in L5, it is likely that some fraction of the V2 L5 input cells were intra-laminar horizontal inputs presynaptic to the V2 starter cells, rather than FB inputs to the V1→V2 cells. Consistent with this interpretation, we also found a small, but larger number of GFP-labeled neurons in L4 (1.7%, n=20 cells) in this case compared to the other two cases. Across the 3 cases, on average 54.3±10.2% of GFP-labeled input cells were located in L5, 4.9±0.6% in L6 and 40.1%±10.1% in L2/3 (**Fig. 4d**), although the L5 bias in the population average is likely due to the intra-V2 inputs to the V2 starter cells in case MK379.

To determine the spatial spread of the V2 FB inputs relative to the V1→V2 starter cells, we measured the distance of each V2 GFP-labeled cell from the center of the V2 injection site, where the V1→V2 starter cells terminated. The spatial spread of the FB inputs was very extensive, reaching up to 7.2 mm away from the injection center (mean max distance across the 3 cases 5.53±1.32mm) (**Fig. 4e**). However, 75% of the FB inputs were located within 1.84±0.38 mm of the injection site. Across the population, the average mean distance ± s.e.m. was 1.37±0.27 mm, and the average median distance ±s.e.m. was 1.14±0.29 mm. When compared to the average spatial spread of the V1→V2 starter cells, the average spread of the V2 FB inputs to these cells was approximately 3.5 times the size of the V1 region to which they projected. These results are consistent with previous reports that V2 FB neurons convey a larger region of visual space to their target V1 cells [40].

The population average ratio of total number of V2 GFP-labeled input neurons to total number of V1→V2 starter cells was 8.7±6.98; the average ratio of V2 FB inputs in each layer to the total number of V1→V2 starter cells pooled across layers was 2.1±1.2 for L2/3, 6.1±5.4 for L5, and 0.3±0.3 for L6 (**Fig. 4f**). The variability in this ratio across cases was due to case MK379, for which there were about 23 total V2 FB input cells per V1 starter cell, while this ratio was about 2:1 for the other two cases. It is likely that the relatively larger number of GFP-labeled neurons in case MK379 was due to additional labeling of intrinsic V2 inputs to the presynaptic V2 starter cells found in this case. This interpretation is consistent with the evidence we present below that neurons receive the largest fraction of their inputs from cells located within the same cortical area.

Higher Extrastriate Cortical Areas Send Monosynaptic FB Inputs to V2→V1, but not V1→V2, Starter Cells

Figure 5 about here

As V1 receives FB connections not only from V2, but also from higher extrastriate cortical areas, including MT, V3, V4, and V6 [18,29,41], to assess whether FB contacts with V1→V2 neurons are area-specific, we searched for fluorescent label throughout cortex anterior to V2, excluding only prefrontal cortex. In the two cases that showed few or no V2→V1 starter cells, we found no GFP-labeled cells in cortex anterior to V2, indicating that FB contacts with V1→V2 neurons are highly area selective. This finding strongly supports the existence of highly specific FF-FB loops. In contrast, in case MK379, which showed a larger fraction of starter cells in V2, we found a total of 7 GFP-labeled cells in extrastriate cortex anterior to V2 (areas V3, V3A and MT), representing 0.6% of the total number of GFP-labeled FB cells in cortex anterior to V1 (**Fig.5**). As this is the only case showing labeled neurons in higher-order extrastriate areas, and the only case with a

significant fraction of starter cells in V2, and because V2 is known to receive FB from areas V3, V3A and MT[18,29,41], in addition to other extrastriate areas, it is highly likely that these GFP-labeled cells in higher extrastriate cortex represent monosynaptic FB inputs to the V2→V1 starter cells. This indicates that a small fraction of FB connections, at least in higher cortical areas, can make direct contacts with FB-projecting neurons in lower-order areas, supporting the existence of cascading FB-to-FB projections connecting higher areas to V1 via a single synapse within each area.

V1→V2 Neurons Receive the Majority of Monosynaptic Cortical Inputs from Within V1

Figure 6 about here

In all three cases, we found many GFP-labeled input cells within all V1 layers, except L1, at distances >400 μm from the injection sites (**Fig. 6a-c**). Within each case, the laminar distribution of V1 inputs closely matched the laminar location of the V1→V2 starter cells. Thus, the majority of V1 inputs were located in L2/3 (**Fig. 6e**), where most of the V1→V2 starter cells were also located (**Fig. 2f**), but in case MK382, where L2/3 and 5 had more similar percentages of starter cells, similar amounts of labeled intra-V1 horizontal inputs were found in both layers (**Fig. 6d**). On average across the population, 46.9±7.3% of V1 inputs arose from L2/3, followed by L5 (23.7±7.5%) (**Fig. 6e**). This is consistent with the well-known prominence of intra-laminar horizontal connections in V1 L2/3 and L5 [42,43]. In all 3 cases, 75% of V1 input cells were located >1mm (mean 1.013±99.7mm) from the closest V1 injection site center, with an average distance of 849.6±69.3 μm and the farthest input cell located 5.71 mm away **(Fig. 6f)**. On average across the population, V1→V2 starter cells received 91.6±3.1% of their total cortical monosynaptic inputs from other V1 cells, with only 8.4±3.1% arising from V2 (**Fig. 6g**). For the different cases, however, this percentage varied with the percent of V1 versus V2 starter cells. Specifically, in cases MK405 and MK382, where 98% and 100%, respectively, of starter cells were located in V1, 93% and 96%, respectively, of their monosynaptic inputs arose from within V1. Instead, in case MK379, where 83% of starter cells were located in V1 and 17% in V2, a lower percent (85%) of GFP-labeled inputs were located in V1, indicating that some fraction of the V2 input cells, in this case, were presynaptic to the V2 starter cells rather than to the V1→V2 cells. These results indicate that monosynaptic FB inputs to V1→V2 neurons are sparse.

Monosynaptic Inputs from the Thalamus

Figure 7 about here

V1 receives subcortical inputs from the lateral geniculate nucleus (LGN) of the thalamus [44,45], as well as the pulvinar [46], a higher-order thalamic nucleus. We asked whether any of these inputs make direct synaptic contacts with V1→V2 cells. In the two cases that showed few or no V2→V1 starter cells, we found no GFP-labeled cells in either the LGN or the pulvinar, indicating that thalamic inputs undergo intra-V1 processing before being relayed to V1 corticocortical output cells. In contrast, in case MK379, which showed a larger percent of starter cells in V2, we found

a small percent of GFP-labeled input cells (0.22% of total) in the LGN (n=14 cells) and pulvinar (n=4 cells; **Fig.7**). In the LGN, 86% of input cells were found in the parvocellular (Parvo) layers, 14% in the magnocellular (Magno) layers, and none in the koniocellular (Konio) layers (**Fig.7a-c, g**). As input cells in the LGN were found only in this case, and this is the only case with a significant fraction of starter cells in V2, and because V2 is known to receive a small number of direct inputs from LGN [47], it is likely that the GFP-labeled cells in the LGN, in this case, represent direct monosynaptic geniculate inputs to the V2→V1 starter cells. This would suggest the existence of direct geniculate inputs onto V2 cells sending FB connections to V1. Because the extrastriate geniculate inputs have been shown to arise primarily, albeit not exclusively, from the Konio layers [47-49], we immunoreacted the LGN for calbindin, a neurochemical marker of the Konio geniculate channel [50]. None of the GFP-labeled cells co-expressed calbindin, suggesting they may not be Konio cells (**Fig. 7a-c**). We found only 4 GFP-labeled cells in the lateral subdivision of the pulvinar (**Fig. 7d-f**), the latter identified as a region of sparser calbindin expression compared to its neighboring inferior subdivision [51]. Based on the same rationale as for the GFP-labeled LGN cells, it is likely that the GFP-labeled cells found in the pulvinar, in this case, represent direct inputs to the starter cells in V2 that send FB to V1.

DISCUSSION

Figure 8 about here

Using TRIO labeling in macaque visual cortex, we have shown that interareal FB connections to V1 selectively contact the V1 projection neurons that are the source of their interareal FF inputs. Specifically, V1 neurons sending FF connections to V2 receive direct monosynaptic inputs from V2 FB neurons, but not from FB neurons in other extrastriate areas that also project to V1. These area-specific monosynaptic FB-to-FF inputs occur in both superficial and deep V1 layers, although our approach did not allow us to determine the differential contribution of superficial and deep layer FB neurons to the V1 termination layers. These direct interareal FB inputs represent only a tiny fraction of the total cortical inputs to V1 cortical projection neurons, which overwhelmingly arise from within V1. We also found evidence for the existence of direct monosynaptic interareal FB-to-FB contacts relaying topdown information from higher extrastriate areas to V1, via a single synapse in V2. Finally, we found sparse direct inputs from the Parvo and Magno LGN layers and lateral pulvinar to V2 L5 neurons sending FB projections to V1 (**Fig. 8**).

It is well established that in the primate visual cortex, most V1 cortical projection neurons send FF projections to only a single area [21-23], but it was unclear whether FB is also area specific and whether it influences FF afferents directly or indirectly. Our results demonstrate that FB connections selectively and monosynaptically contact neurons that are the source of their FF inputs. This is in contrast with results from mouse V1, where about 80-88% of FF projection neurons project to one or two higher visual areas [19,52], but only about 50% of their monosynaptic FB contacts arise from the same areas to which they project [19]. Moreover, recent evidence suggests that in mouse a bias to form area-specific monosynaptic excitatory FF-FB loops may be limited to deep layer neurons [20], while our results in monkey demonstrate area-selective FB-to-FF contacts in both V1 superficial and deep layers. These findings strongly support the existence of area-, and thus, stream-specific, FF-FB loops in primate cortex.

Our findings support several theories advocating looped computations between FF and FB connections [8-16]. The specific nature of the computations performed by these loops vary with the specific theory. For example, in predictive coding theory, FB signals represent a prediction of the external world, based on sensory data and prior experience; this prediction is compared with incoming sensory data, and the prediction error, carried by FF-projecting "error units", ascends up the cortical hierarchy and refines the higher level predictions [8,9,53]. In terms of their architecture, predictive coding schemes require both excitatory and inhibitory looped interactions of FB inputs with lower-level "error units" to signal mismatches between predictions and sensory inputs [54,55]. Moreover, these looped interactions must occur between FF and FB units encoding similar features. Our findings of area-specific monosynaptic FB contacts with FF-projecting neurons could provide an anatomical substrate for excitatory FB interactions with the lower-level error units (so called "negative error units") required by predictive coding [55]. Alternatively, direct FB-to-FF contacts could underlie the "precision" FB signals of predictive coding models[54,55]. In the latter, the precision FB circuit is distinct from the prediction circuit, and provides a modulatory or gating FB signal that sets the weight or precision of the prediction error. However, an additional key component of predictive coding models is the inhibitory FB interaction with the lower-level error units (so called "positive error units"), which requires FB contacts with inhibitory neurons. Moreover, experimentally FB has been shown to cause both facilitation and suppression of neural activity in lower-level areas [56-58]. Thus, the direct FB-to-FF connections we have found here could underlie the facilitatory effects of FB, but direct or indirect contacts with inhibitory neurons are necessary to mediate the FB suppressive effects found experimentally and postulated by predictive coding. Indeed, direct FB contacts with inhibitory neurons have been demonstrated in both mouse [59-61] and primate [62] visual cortex. Therefore, monosynaptic FB-FF contacts likely represent just one of several motifs of FB connectivity in primate cortex.

Our approach did not allow us to determine whether the V1→V2 neurons receiving the direct FB contacts directly target the same V2 neurons that are the source of their FB input. Notably, these direct FF-FB contacts are not required by predictive coding schemes. To the contrary, several of the proposed schemes require that FF inputs from lower-level error units indirectly affect their looped prediction FB units, via contacts with local neurons making recurrent connections with each other [54,63]. This intra-areal recurrent processing between local expectation units gives rise to, maintains, and refines the internal predictions, which are then passed on to the FB units for relay to lower-level areas. Moreover, the termination of FF pathways from V1 predominantly to L4 and lower 3 of V2, and the origin of V2 FB pathways in layers 2/3 and 5/6 [29] would make direct FF-to-FB contacts less probable than indirect ones.

A different theory postulates that fast recurrent FB-FF processing between adjacent hierarchically-organized areas serves to facilitate object recognition, particularly when incoming sensory inputs are ambiguous, degraded or noisy [12]. In these models, these local FB signals are fast, operating during the initial FF process. The area-specific monosynaptic FB-to-FF contacts we have found here represent an ideal anatomical substrate for fast and specific facilitatory FB modulation of incoming FF signals, and are also consistent with evidence that FB acts on the early part of the FF-driven response [64].

We found FB inputs to V1→V2 neurons arise from a cortical region about 3.5 times the size of their V1 target zone, indicating FB neurons convey a larger region of visual space to their target V1 cells. This is consistent with previous reports that V2 FB connections to a V1 column in macaque extend on average 6.1-6.4 mm (up to 9mm) in diameter, corresponding in visual field

coordinates to about 4 times the size of the aggregate receptive fields of their target V1 cells [40]. Similar results were recently reported for FB connections in mouse visual cortex[65], suggesting that a feature of FB connections conserved across species is their ability to convey information from distant visual field locations to their postsynaptic neuronal targets. This feature has been proposed to underlie contextual modulations from outside the classical receptive field [66].

Our results demonstrate that FF-projecting V1 neurons only receive a small fraction of their direct long-range (>400μm) cortical inputs from FB neurons, the majority of which, instead, arise from neurons within V1, particularly in L2/3 and L5, where intralaminar horizontal connections are known to be most prominent [42]. While it is well established that cortical neurons receive the majority (79%) of their inputs from neurons within the same cortical area [67], this is the first demonstration in primate cortex that this connectivity rule also applies specifically to cortical projection neurons.

At least in the dorsal stream of visual processing, we found evidence for a second motif of FB connectivity, namely inter-areal FB-to-FB neuron contacts (**Fig. 8**). These chains of FB connections may serve to convey fast FB modulations, possibly related to the processing of object motion, from higher cortical areas V3, V3A and MT to V1, via V2. However, given that area V3 and MT also send direct inputs to V1, these FB inputs to V2 may serve to specifically modulate V2 FB inputs to V1. These FB-to-FB circuits represent a sparse projection, as we only found a total of 7 neurons in higher extrastriate areas projecting to 11 L5 V2→V1 cells.

The same V2→V1 FB cells that received direct FB inputs from higher extrastriate areas of the dorsal stream, also received direct FF inputs from the LGN and lateral pulvinar (**Fig. 8**). We found GFP-labeled neurons in the LGN and pulvinar only in the one case that showed labeled starter cells in V2 L5, suggesting these thalamic inputs target, and thus can directly influence the activity of, these V2→V1 L5 FB neurons. It is well known that V2 receives a sparse direct projection from the LGN, which has been postulated to be part of a retino-colliculo-thalamic pathway to extrastriate cortex [47,67]. However, while this projection, as well as direct geniculate projections to other extrastriate areas, arise predominantly from calbindin-positive or CaMKII-positive Konio geniculate neurons terminating in L4 and 5 [47-49], here we find these direct LGN-to-V2 FB contacts arise from calbindin-negative cells in the Parvo and Magno LGN layers. While lack of calbindin immunoreactivity suggests neurons giving rise to these projections may not belong to the Konio system, it has been noted that this system is heterogeneous and also includes neurons that are calbindin and CaMKII-negative [48,49]. We cannot exclude that at least some of the Parvo LGN inputs were, instead, presynaptic to the starter V1 cells in L4A, as Parvo-to-L4A projections exist [68]; this would indicate the existence of direct geniculate inputs to L4A output cells. However, we believe this is unlikely, because two of our cases with starter cells in L4A, but few or no starter cells in V2, showed no labeled input cells in the LGN. Similarly, as the lateral pulvinar in addition to V2 also projects to L1-2 of V1[46,69], it is possible, although unlikely, that the pulvinar inputs we observed here were instead presynaptic to the apical dendrites of the starter cells in V1 L2-4B or L5. This would suggest that the pulvinar can directly affect the activity of V1 cortical output cells. Finally, as Magno afferents only terminate in V1 L4C and 6, and there were no starter cells in these V1 layers, it is unlikely the sparse Magno inputs found in our study represent direct inputs to V1 output cells.

ONLINE METHODS

We performed monosynaptic input tracing or TRIO to label monosynaptic inputs to V1→V2 neurons (starter cells) in macaque monkey. The method consisted of targeting injections of 3 different viral vectors to V1 or V2, identified *in vivo* by intrinsic signal optical imaging (OI). Resulting labeled starter cells and input cells were mapped throughout V1, V2, extrastriate cortex and thalamus, and their laminar and tangential distributions were analyzed quantitatively.

Animals

We made a total of 25 viral injections in five adult female cynomolgus macaque monkeys (*Macaca fascicularis)*. Three animals were used for regular TRIO experiments and 2 for control experiments. All procedures involving animals were approved by the Institutional Animal Care and Use Committee of the University of Utah and conformed to the guidelines set forth by the USDA and NIH.

Surgical Procedures

Animals were pre-anesthetized with ketamine (10 mg/kg, i.m.). An i.v. catheter was inserted, and the animals were intubated with an endotracheal tube, placed in a stereotaxic apparatus, and artificially ventilated. Anesthesia was maintained with isofluorane (1–2.5%) in 100% oxygen, and end tidal CO_2, blood oxygenation level, electrocardiogram, and body temperature were monitored continuously. I.V. fluids were delivered at a rate of 5/cc/kg/hr. The scalp was incised, a large craniotomy and durotomy (about 15-20 mm mediolaterally and 6-8 mm anteroposteriorly) were made to expose the lunate sulcus, area V2 and parts of V1 (e.g. **Fig. 1b**). A clear sterile silicone artificial dura was placed on the cortex, and the craniotomy was filled with a sterile 3% agar solution and sealed with a glass coverslip glued to the skull with Glutures (Abbott Laboratories, Lake Bluff, IL). On completion of surgery, isoflurane was turned off and anesthesia was maintained with sufentanil citrate (5–10 μg/kg/h, i.v.). The pupils were dilated with a short-acting topical mydriatic agent (tropicamide), the corneas protected with gas-permeable contact lenses, the eyes refracted, and optical imaging was started (see below). Once the V1/V2 border was functionally identified (1-4 hrs. of imaging), the glass coverslip, agar and artificial dura were removed, and 2-3 injections of AAV9 vectors (see below) were made in V1 using surface blood vessels as guidance. On completion of the injections, new artificial dura was placed on the cortex, the native dura was sutured over the artificial dura, the craniotomy was filled with Gelfoam and sealed with sterile parafilm and dental cement, the skin was sutured, and the animal was recovered from anesthesia. Animals survived 21-24 days post-injections, and then were prepared for a second surgical procedure and anesthetized with isofluorane as described above. The scalp was re-incised at the same site as the prior incision, the artificial dura was removed, and 1-2 injections of the CAV2 vector (see below) were made in V2, using as guidance the surface blood vessels and functional OI maps obtained in the first surgical procedure. The animals were recovered as described above, and after a 2-11-day survival time underwent a third surgical procedure during which multiple injections of the RV*dG* vector (see below) were made at the same locations as the previously made AAV injections in V1. Animals survived an additional 9-12 days, during which a terminal 2-3 day OI experiment was performed to obtain additional functional maps. At the conclusion of the OI experiment the animal was sacrificed with Beuthanasia (0.22 ml/kg, i.v.) and

perfused transcardially with saline for 2–3 min, followed by 4% paraformaldehyde (PFA) in 0.1M phosphate buffer for 20 min.

Optical Imaging

Acquisition of intrinsic signals was performed under red light illumination (630 nm) during the first survival surgery and, then, again during a terminal procedure, using the Imager 3001 and VDAQ software (Optical Imaging Ltd, Israel). We imaged for orientation and retinotopy, as these functional maps allow identification of the V1/V2 border. Orientation maps were obtained by presenting full-field, high contrast (100%), pseudorandomized, achromatic drifting square-wave gratings of eight different orientations at 1.0-2.0 cycles/° spatial frequency, moving back and forth at 1.5 or 2°/sec in directions perpendicular to the grating orientation. Responses to the same orientations were averaged across trials, baseline subtracted, and difference images obtained by subtracting the responses to two orthogonal oriented pairs. V2 can be identified by larger orientation domains compared to V1, and the characteristic "stripy" pattern of orientation domains (e.g. **Fig. 1b** right). Retinotopic maps were obtained by subtracting responses to monocularly presented oriented gratings occupying complementary adjacent strips of visual space, i.e. masked by 0.5-1° gray strips repeating every 1-2°, with the mask reversing in position in alternate trials. The V1/V2 border can be identified in these maps by the presence of stripes of activity in V1, which are absent in V2 (using the specific stimulus parameters indicated above, which are optimized for V1, but not V2). In each case, reference images of the surface vasculature were taken under green light (546 nm) illumination, and used *in vivo* as reference to position pipettes for viral vector injections (e.g. **Fig. 1b** Left), and post-mortem to align the *in vivo* maps with histological tissue sections.

Injections of Viral Vectors

For TRIO experiments, we made a total of 21 injections of 4 different viral constructs in 3 macaques (MK379, MK382, MK405). The viral vectors were: AAV9-CAG-FLEX-TVAmCherry (titer: $4.69x10^{13}$ GC/ml; Salk Institute Viral Core GT3), AAV9-CAG-FLEX-oG-WPRE (titer: 3.52×10^{13} GC/ml; Salk Institute Viral Core GT3), E1-deleted-CAV2-CMV-Cre-SV40polyA (titer: $4.6x10^{12}$ pp/ml; Montpellier Vector Platform, CNRS, France) and EnvA-RV*d*G-eGFP (titer range: $4.69x10^{7}$- $5.45x10^{8}$ TU/ml; Salk Institute Viral Core GT3). All viruses were slowly pressure injected at a rate of 6-15nl/min, using a picospritzer (World Precision Instruments, FL, USA) and glass micropipettes (25-50 µm inner diameter). The two AAV9 vectors were mixed at 1:1 or 3:7 ratio and loaded into the same glass micropipette, and 2-3 injections of the mixture were made into V1, 1-1.3mm posterior to the V1/V2 border and spaced mediolaterally (i.e. in a row parallel to the V1/V2 border) 1-1.1 mm apart (**Fig. 1b**). These injections were aimed at involving all V1 layers by pressure ejecting half of the total volume at a cortical depth of 800-1200 µm from the pial surface and, after a 5-10 min pause, retracting the pipette to a depth of 400-600 µm and ejecting the remaining volume. The pipette was left in place for an additional 5-10 min before being retracted from the brain, to avoid backflow of solution. After about 21 days, 1-2 injections of the CAV2 vector were made into V2, 1-1.1 mm anterior to the V1/V2 border and, when 2 injections were made, they were spaced 200-300 µm anteroposteriorly (**Fig. 1b)**. V2 injections were made as described above for the V1 injections, but were aimed at cortical L4-6 (depths 700 µm and

1,000 μm). After 2-11 days survival, 2-3 injections of the RV*d*G vector were made into V1 at the same locations and depths as the previously made AAV injections, whose location relative to the surface vasculature had been recorded onto the *in vivo* images obtained during the first surgery. The larger number of injections in V1 allowed us to achieve a larger coverage with the AAV and RV*d*G vectors, to ensure that at least one of these injections was retinotopically matched to the location of the V2 injection site. Survival times were optimized to achieve maximal expression of each vector in primate cortex, while minimizing its potential toxicity. Injection parameters (volumes, numbers, depths) and inter-injection survival times for each animal are reported in **Supplementary Table 1**.

Control Injection Cases

A total of 4 viral injections were made in 2 additional animals (MK380, MK381) for control experiments, to determine the amount and extent of Cre-independent GFP expression caused by TVA leak. In each animal, one injection each of the AAV9 and RV*d*G vectors were made in the motor cortex, using the same viral constructs, injection parameters, depth locations and survival times (**Supplementary Table 1**) as used for the regular TRIO experiments, but in these control experiments the CAV2-Cre injection was omitted.

Histology

Areas V1 and V2 were separated from the rest of the visual cortex, by making a cut along the fundus of the lunate sulcus. The block was post-fixed for 1 hour in 4% PFA between glass slides, to gently flatted the cortex parallel to the imaged area, cryoprotected in 30% sucrose, and frozen-sectioned at 40 μm on a sliding microtome in a plane tangential to the imaged surface of V1 and V2. Sections were wet-mounted, scrutinized for fluorescent label and, selected sections containing label were imaged for fluorescent GFP and mCherry label. After imaging, every third section was reacted on the glass slide for cytochrome oxidase (CO), to reveal layers and areal boundaries, and the sections were re-imaged under bright field illumination.

The remainder of the brain, with the frontal pole removed, was post-fixed overnight in 4% PFA, cryoprotected and sectioned sagittally at 70 μm. A full series of sections was wet-mounted and imaged for fluorescent label. Sections containing fluorescent label were stained for myelin using the Gallyas method [70], to aid in the identification of extrastriate areas and areal boundaries, and stained for fluorescent Nissl to identify cortical layers and subcortical nuclei. Furthermore, to identify the pulvinar subdivisions and the koniocellular layers of the LGN, selected sections containing fluorescent label were immunoreacted for Calbindin as follows. Sections were incubated in primary antibody (1:5000 monoclonal mouse anti-Calbindin D-28k; Swant, Switzerland) for 72 hours at 4°C, and then reacted with a secondary antibody tagged to a near-infrared fluorophore (1:200 donkey anti-mouse IgG-AF647; Jackson ImmunoResearch, PA, USA).

Data Analysis

Label Imaging

We searched for fluorescent label every section throughout the cortex (except for the prefrontal cortex) and thalamus. We then imaged at regular intervals (2 every 3 sections) two full series of sections throughout the regions containing labeled cells. Tissue sections were simultaneously imaged for both GFP and mCherry fluorescence, and the sections immunoreacted for Calbindin and stained for Nissl were additionally imaged for Alexa 647 and DAPI, respectively. Imaging was performed on a Zeiss Axio Imager.Z2 fluorescent microscope connected to an Apotome.2, using a 10X objective and an Axiocam 506 mono camera (Zeiss, Germany). Image files were created and analyzed using Zen 2.6 Blue Software (Zeiss, Germany). Sections were imaged using uniform camera exposure times and LED intensity. Imaged sections were scrutinized for fluorescent label and the regions containing double-labeled (green and red) starter cells were re-imaged at higher magnification, using a 20x objective and the Apotome to obtain z-stacks in 1-2 μm z-steps, so as to verify cells classified as double-labeled. CO and Gallyas stainings were imaged under bright field illumination, using the same microscope and a 10x objective. All images were post-processed in Zen using the Stitching algorithm to align individual image tiles and minimize tiling artifacts. Images used for figures were exported directly from Zen files, and brightness or contrast were uniformly increased or decreased in Adobe Photoshop across the entire image in each channel.

Cell Counts

Imaged sections were aligned in a sequential stack through the depth of the cortex (for tangentially-sectioned V1/V2 blocks), or in a mediolateral stack (for sagittally-sectioned tissue) using Adobe Photoshop, by registering the radial blood vessels. The aligned image stacks were then transferred to Neurolucida Software (Microbrightfield Bioscience, VT, USA) for cell plotting and counting, and for drawing layer boundaries based on CO and Nissl stains. For each section containing label, we plotted and counted all GFP-labeled (green) input cells (excluding only GFP-labeled cells in V1 located at distances <400 μm from each injection site center), and all double-labeled (yellow) starter cells. For V1 and V2, we imaged and counted two full series of sections, while for thalamus and the rest of the cortex we counted every labeled cell in every section that contained label. We defined "input" cells as cells exclusively labeled with GFP showing morphological and size characteristics of neurons. "Starter" cells were defined as somata expressing both GFP and mCherry (double-labeled) in the same imaging z-plane, with the two labels perfectly overlapped. Since GFP and TVAmCherry are differently distributed inside neurons, the former filling the soma and the latter binding to the cell membrane, we allowed for the possibility that GFP and mCherry-labeled cells did not show identical shapes. Each cell was additionally assigned a layer location and number of cells in each layer was determined.

Measurements of Cell Distances

To quantify the spatial spread of the inputs to V1 starter cells within V1, we measured the distance of each V1 GFP-labeled input cell from the center of the nearest V1 injection site containing

labeled starter cells anywhere along the injection track. We chose to measure the cells' distance to the nearest injection site, rather than to V1 starter cells, because our method does not allow us to determine to which starter cell each input cell projects. For V2 input cells, distance was measured from the nearest V2 injection site center, as this is where the terminals of the V1 starter cells are located, as also indicated by the presence of red axonal label (e.g. **Fig. 3b,** and middle panel in **Fig. 4b**). We also measured the distance of each starter cell in V1 and V2 from the center of the nearest injection site within the same area, to determine the spatial extent of the starter cell label (**Figs. 2g, 3e**). Injection sites were identified by aligning the top histological sections containing the surface blood vessels to the *in vivo* images of the surface vasculature, taken under green light illumination during OI, onto which injection site locations had been marked (**Fig. 1b** Left). Injection site locations were then confirmed as points of damage, or discolorations in CO staining, across multiple serial sections (e.g. top panels in **Figs. 2a-b, 3a, 4a-b**), and their centers were marked in each section. We did not measure distances from injection sites for labeled cells in the thalamus or extrastriate cortex, which were all considered extra-V1 long-range inputs.

Quantification

For each case, within each cortical area we counted the number of input and starter cells in each layer and estimated the percentage of total input or starter cell counts, respectively, in each layer (**Figs. 2e,3d,4c,6d**). We then averaged these percentages across the 3 cases for each layer and estimated the s.e.m. (**Figs. 2f,4d,6e**).

Cell distance data was plotted as histograms of the number of cells as a function of distance from the nearest injection site, as well as violin plots to illustrate the probability density distribution of distances (**Figs. 2g,3e,4e,6f**). For each case, we also calculated a ratio of the number of V2 input cells in each V2 layer to the total number of V1 starter cells (across all V1 layers), and then averaged these ratios across cases by V2 layer (**Fig. 4f**). We divided by the total number of V1 starter cells, as our method does not allow us to determine to which layers the V2 FB cells project. Finally, for each case we estimated the percent of total V1 and V2 input cells that arose from V2 versus V1, and then averaged those values across cases (**Fig. 6g**).

ACKNOWLEDGMENTS

We thank Kesi Sainsbury for technical assistance, Dr. Sam Merlin for help in one experiment, Matthew Spurrier, Porter Babcock, Gabriella Rasmussen, and Alexander Ingold for help with imaging tissue sections. Supported by grants from the National Institute of Health (R01 EY026812, R01 EY019743, BRAIN U01 NS099702), the National Science Foundation (IOS 1755431, EAGER 1649923), and The University of Utah Neuroscience Initiative, to A.A., a grant from Research to Prevent Blindness, Inc. and a core grant from the National Institute of Health (EY014800) to the Department of Ophthalmology, University of Utah.

AUTHOR CONTRIBUTIONS

Conceptualization: all authors. Investigation: all authors. Data Analysis: C.S., J.B. Writing-Original Draft: C.S., A.A. Writing–Review/Editing: all authors. Visualization: C.S. Supervision & Funding Acquisition: A.A.

COMPETING INTERESTS STATEMENT

The authors declare no competing interests.

REFERENCES

1. Van Essen, D.C. & Maunsell, J.H.R. Hierarchical organization and functional streams in the visual cortex. *Trends Neurosci.* **6**, 370-375 (1983).

2. Markov, N.T. & Kennedy, H. The importance of being hierarchical. *Curr. Opin. Neurobiol.* **23**, 187-194 (2013).

3. Ungerleider, L.G. & Mishkin, M. Two cortical visual systems. In *Advances in the analysis of visual behavior* (ed. D.J. Ingle, J.W. Mansfield & M.A. Goodale) 549-586 (MIT Press, Cambridge, 1982).

4. Nassi, J.J. & Callaway, E.M. Parallel processing strategies of the primate visual system. *Nat. Rev. Neurosci.* **10**, 360-372 (2009).

5. Hubel, D.H. & Wiesel, T.N. Receptive fields, binocular interaction and functional architecture in the cat's visual cortex. *J. Physiol. (Lond.)* **160**, 106-154 (1962).

6. Marr, D. *Vision. A computational investigation into the human representation and processing of visual information.* (Freeman, W.H. and Company, 1982).

7. DiCarlo, J.J., Zoccolan, D. & Rust, N.C. How does the brain solve visual object recognition? *Neuron* **73**, 415-434 (2012).

8. Mumford, D. On the computational architecture of the neocortex. II. The role of cortico-cortical loops. *Biol. Cybern.* **66**, 241-251 (1992).

9. Rao, R.P. & Ballard, D.H. Predictive coding in the visual cortex: a functional interpretation of some extra-classical receptive-field effects. *Nat. Neurosci.* **2**, 79-87 (1999).

10. Friston, K. The free-energy principle: a unified brain theory? *Nat. Rev. Neurosci.* **11**, 127-138 (2010).

11. Lee, T.S. & Mumford, D. Hierarchical Bayesian inference in the visual cortex. *J. Opt. Soc. Am. A Opt. Image. Sci. Vis.* **20**, 1434-1448 (2003).

12. Wyatte, D., Jilk, D.J. & O'Reilly, R.C. Early recurrent feedback facilitates visual object recognition under challenging conditions. *Front Psychol* **5**, 674 (2014).

13. Rolls, E.T. The representation of information in the temporal lobe visual cortical areas of macaques. In *Advanced neural computers* (ed. R. Eckmiller) 69-78 (Elsevier, New York, Amsterdam, 1990).

14. Poggio, T. A theory of how the brain might work. in *Proc. Cold Spring Harbor Symp.* (1990).

15. Deacon, T. Holism and associationism in neuropsychology: an anatomical synthesis. In

Integrating theory and practice in clinical neuropsychology (ed. E. Perecman) (Erlbaum, Hillsdale, NJ, 1988).

16. Carpenter, G. & Grossberg, S. A massively parallel architecture for a self-organizing neural pattern recognition machine. *Comp. Vision Graphics Image Proc.* **37**, 54-115 (1987).

17. Felleman, D.J. & Van Essen, D.C. Distributed hierarchical processing in the primate cerebral cortex. *Cereb. Cortex* **1**, 1-47. (1991).

18. Markov, N.T.*, et al.* Anatomy of hierarchy: feedforward and feedback pathways in macaque visual cortex. *J. Comp. Neurol.* **522**, 225-259 (2014).

19. Kim, E.J.*, et al.* Extraction of Distinct Neuronal Cell Types from within a Genetically Continuous Population. *Neuron* **107**, 1-9 (2020).

20. Young, H., Belbut, B., Baeta, M. & Petreanu, L. Laminar-specific cortico-cortical loops im mouse visual cortex. *BioRxiv* **doi.org/10.1101/773085** (2019).

21. Bullier, J., Kennedy, H. & Salinger, W. Branching and laminar origin of projections between visual cortical areas in the cat. *J. Comp. Neurol.* **228**, 329-341 (1984).

22. Sincich, L.C. & Horton, J.C. Independent projection streams from macaque striate cortex to the second visual area and middle temporal area. *J. Neurosci.* **23**, 5684-5692. (2003).

23. Ferrer, J.M., Kato, N. & Price, D.J. Organization of association projections from area 17 to areas 18 and 19 and to suprasylvian areas in the cat's visual cortex. *J. Comp. Neurol.* **316**, 261-278 (1992).

24. Rockland, K.S. & Van Hoesen, G.W. Direct temporal-occipital feedback connections to striate cortex (V1) in the macaque monkey. *Cereb. Cortex* **4**, 300-313 (1994).

25. Kennedy, H. & Bullier, J. A double-labeling investigation of the afferent connectivity to cortical area V1 and V2 of the macaque monkey. *J. Neurosci.* **5**, 2815-2830 (1985).

26. Rockland, K.S. & Knutson, T. Feedback connections from area MT of the squirrel monkey to areas V1 and V2. *J. Comp. Neurol.* **425**, 345-368 (2000).

27. Stettler, D.D., Das, A., Bennett, J. & Gilbert, C.D. Lateral connectivity and contextual interactions in macaque primary visual cortex. *Neuron* **36**, 739-750. (2002).

28. Maunsell, J.H.R. & Van Essen, D.C. The connections of the middle temporal visual area (MT) and their relationship to a cortical hierarchy in the macaque monkey. *J. Neurosci.* **3**, 2563-2586. (1983).

29. Rockland, K.S. & Pandya, D.N. Laminar origins and terminations of cortical connections of the occipital lobe in the Rhesus monkey. *Brain Res.* **179**, 3-20 (1979).

30. Federer, F., Ta'afua, S., Merlin, S. & Angelucci, A. Stream-specific feedback inputs to the primate primary visual cortex. Preprint at https://www.biorxiv.org/content/10.1101/2020.1103.1104.977264v977261 (2020).

31. Shmuel, A., *et al.* Retinotopic axis specificity and selective clustering of feedback projections from V2 to V1 in the owl monkey. *J. Neurosci.* **25**, 2117-2131 (2005).

32. Callaway, E.M. & Luo, L. Monosynaptic Circuit Tracing with Glycoprotein-Deleted Rabies Viruses. *J. Neurosci.* **35**, 8979-8985 (2015).

33. Schwarz, L.A., *et al.* Viral-genetic tracing of the input-output organization of a central noradrenaline circuit. *Nature* **524**, 88-92 (2015).

34. Kim, E.J., Jacobs, M.W., Ito-Cole, T. & Callaway, E.M. Improved monosynaptic neural circuit tracing using engineered rabies virus glycoproteins. *Cell Reports* **http://dx.doi.org/10.1016/j.celrep.2016.03.067** (2016).

35. Bru, T., Salinas, S. & Kremer, E.J. An update on canine adenovirus type 2 and its vectors. *Viruses* **2**, 2134-2153 (2010).

36. Sincich, L.C., Jocson, C.M. & Horton, J.C. V1 interpatch projections to V2 thick stripes and pale stripes. *J. Neurosci.* **30**, 6963-6974 (2010).

37. Federer, F., *et al.* Four projections streams from primate V1 to the cytochrome oxidase stripes of V2. *J. Neurosci.* **29**, 15455-15471 (2009).

38. Green, F., *et al.* Axonal transport of AAV9 in nonhuman primate brain. *Gene Ther.* **23**, 520-526 (2016).

39. Lavin, T.K., Jin, L. & Wickersham, I.R. Monosynaptic tracing: a step-by-step protocol. *J. Chem. Neuroanat.* **102**, 101661 (2019).

40. Angelucci, A., *et al.* Circuits for local and global signal integration in primary visual cortex. *J. Neurosci.* **22**, 8633-8646. (2002).

41. Rockland, K.S. & Pandya, D.N. Cortical connections of the occipital lobe in the rhesus monkey: interconnections between areas 17, 18, 19 and the superior temporal sulcus. *Brain Res.* **212**, 249-270 (1981).

42. Lund, J.S., Angelucci, A. & Bressloff, P.C. Anatomical substrates for functional columns in macaque monkey primary visual cortex. *Cereb. Cortex* **13**, 15-24 (2003).

43. Rockland, K.S. & Lund, J.S. Intrinsic laminar lattice connections in primate visual cortex. *J. Comp. Neurol.* **216**, 303-318. (1983).

44. Hendrickson, A.E., Wilson, J.R. & Ogren, M.P. The neuroanatomical organization of pathways between the dorsal lateral geniculate nucleus and visual cortex in Old World and New

World primates. *J. Comp. Neurol.* **182**, 123-136 (1978).

45. Blasdel, G.G. & Lund, J.S. Terminations of afferent axons in macaque striate cortex. *J. Neurosci.* **3**, 1389-1413 (1983).

46. Rezak, M. & Benevento, L.A. A comparison of the organization of the projections of the dorsal lateral geniculate nucleus, the inferior pulvinar and adjacent lateral pulvinar to primary visual cortex (area 17) in the macaque monkey. *Brain Res.* **167**, 19-40 (1979).

47. Bullier, J. & Kennedy, H. Projection of the lateral geniculate nucleus onto cortical area V2 in the macaque monkey. *Exp. Brain Res.* **53**, 168-172 (1983).

48. Rodman, H.R., Sorenson, K.M., Shim, A.J. & Hexter, D.P. Calbindin immunoreactivity in the geniculo-extrastriate system of the macaque: implications for heterogeneity in the koniocellular pathway and recovery from cortical damage. *J. Comp. Neurol.* **431**, 168-181 (2001).

49. Sincich, L.C., Park, K.F., Wohlgemuth, M.J. & Horton, J.C. Bypassing V1: a direct geniculate input to area MT. *Nat. Neurosci.* **7**, 1123-1128 (2004).

50. Diamond, I.T., Fitzpatrick, D. & Schmechel, D. Calcium binding proteins distinguish large and small cells of the ventral posterior and lateral geniculate nuclei of the prosimian galago and the tree shrew (Tupaia belangeri). *Proc. Natl. Acad. Sci. U. S. A.* **90**, 1425-1429 (1993).

51. Adams, M.M., Hof, P.R., Gattass, R., Webster, M.J. & Ungerleider, L.G. Visual cortical projections and chemoarchitecture of macaque monkey pulvinar. *J. Comp. Neurol.* **419**, 377-393 (2000).

52. Han, Y.*, et al.* The logic of single-cell projections from visual cortex. *Nature* **556**, 51-56 (2018).

53. Friston, K. & Kiebel, S. Predictive coding under the free-energy principle. *Philos. Trans. R .Soc. Lond. B Biol. Sci.* **364**, 1211-1221 (2009).

54. Shipp, S. Neural Elements for Predictive Coding. *Front. Psychol.* **7**, 1792 (2016).

55. Keller, G.B. & Mrsic-Flogel, T.D. Predictive Processing: A Canonical Cortical Computation. *Neuron* **100**, 424-435 (2018).

56. Nurminen, L., Merlin, S., Bijanzadeh, M., Federer, F. & Angelucci, A. Top-down feedback controls spatial summation and response amplitude in primate visual cortex. *Nature Commun.* **9**, 2281 (2018).

57. McAdams, C.J. & Reid, C.R. Attention modulates the responses of simple cells in monkey primary visual cortex. *J. Neurosci.* **25**, 11023-11033 (2005).

58. Vidyasagar, T.R. Gating of neuronal responses in macaque primary visual cortex by an attentional spotlight. *Neuroreport* **9**, 1947-1952 (1998).

59. Shen, S.*, et al.* Distinct organization of two cortico-cortical feedback pathways. *BioRxiv* **doi.org/10.1101/2020.02.27.968792** (2020).

60. Yang, W., Carrasquillo, Y., Hooks, B.M., Nerbonne, J.M. & Burkhalter, A. Distinct balance of excitation and inhibition in an interareal feedforward and feedback circuit of mouse visual cortex. *J. Neurosci.* **33**, 17373-17384 (2013).

61. Zhang, S.*, et al.* Long-range and local circuits for top-down modulation of visual cortex processing. *Science* **345**, 660-665 (2014).

62. Anderson, J.C. & Martin, K.A.C. The synaptic connections between cortical areas V1 and V2 in macaque monkey. *J. Neurosci.* **29**, 11283-11293 (2009).

63. Bastos, A.M.*, et al.* Canonical microcircuits for predictive coding. *Neuron* **76**, 695-711 (2012).

64. Hupé, J.M.*, et al.* Feedback connections act on the early part of the responses in monkey visual cortex. *J. Neurophysiol.* **85**, 134-145. (2001).

65. Marques, T., Nguyen, J., Fioreze, G. & Petreanu, L. The functional organization of cortical feedback inputs to primary visual cortex. *Nat. Neurosci.* **21**, 757-764 (2018).

66. Angelucci, A.*, et al.* Circuits and mechanisms for surround modulation in visual cortex. *Ann. Rev. Neurosci.* **40**, 425-451 (2017).

67. Markov, N.T.*, et al.* Weight consistency specifies regularities of macaque cortical networks. *Cereb Cortex* **21**, 1254-1272 (2011).

68. Lund, J.S. Organization of neurons in the visual cortex, area 17, of the monkey (Macaca mulatta). *J. Comp. Neurol.* **147**, 455-496 (1973).

69. Lund, J.S., Hendrickson, A.E., Ogren, M.P. & Tobin, E.A. Anatomical organization of primate visual cortex area VII. *J. Comp. Neurol.* **202**, 19-45 (1981).

70. Gallyas, F. Silver staining of myelin by means of physical development. *Neurol. Res.* **1**, 203-209. (1979).

FIGURE LEGENDS

Figure 1. Monosynaptic input tracing in macaque visual cortex: experimental procedure.

(a) Viral injection timeline and experimental design. *Left*: V1→V2 neurons express mCherry (*red cells*), TVA and oG, after double infection with AAV9-vectors (injected in V1) and CAV2-Cre (injected in V2). *Right*: After additional infection with EnvA-RV*dG*-eGFP (injected at the same V1 sites as AAV9), V1→V2 neurons previously infected with AAV9 additionally express eGFP, becoming double-labeled (*yellow starter cells*). After trans-synaptic RV*dG*-eGFP infection, V1 and V2 cells presynaptic to the V1 starter cells express eGFP (*green cells*). Cells that are not co-infected with both CAV2 and AAV9 remain unlabeled. **(b)** *In vivo* OI of V1 and V2 in one example case (MK405). *Left:* Image of the cortical surface vasculature encompassing V1 and V2. *Solid white contour:* V1-V2 border. The surface vasculature is used as reference to target viral injections to matching retinotopic positions in V1 and V2. *Red, green and white spots:* locations of AAV9, RV*dG* and CAV2 injections, respectively. *Right*: Difference orientation map of V1 and V2 obtained by subtracting responses to achromatic luminance gratings of one orientation from gratings of the orthogonal orientation. V2 can be distinguished from V1 due to its "stripy" pattern and larger orientation domains. M: Medial; P: posterior. Scale bar: 1 mm. **(c)** Case MK405. Image of the viral injection sites through V1 layers 2/3 taken under mCherry and GFP fluorescence, and then merged. *Red cells*: V1→V2 neurons co-infected with CAV2 and AAV9 vectors, but not with RV*dG* vector. *Yellow cells:* starter V1→V2 cells double-labeled due to triple infection with all 3 viral vectors. *Green cells:* cells sending monosynaptic input to the starter V1→V2 cells (but some local V1 green label is due to TVA "leak" – see Results and **Extended Data Fig. 1**). Scale bar: 100 μm. Cells in the *boxed region* are shown at higher magnification in (d) **(d)** Higher magnification of 3 starter V1→V2 cells (*arrowheads*) shown under mCherry (*Left*) or GFP fluorescence (*Middle*), and merged (*Right*). Scale bar: 50 μm.

Figure 2. V1→V2 starter cells.

(a) Case MK405. Image of a single tangential section through V1 L2/3 stained for CO (*Top*) after being imaged for mCherry and GFP fluorescence (*Bottom*). The merged channel shows starter V1→V2cells (*yellow*). *Arrows* point to the V1 injection sites in both sections, which are recognizable as discoloration in CO staining. The region inside the *white box* is shown at higher magnification in panel (c). **(b)** Image of a single tangential section through V1 L4C-6 stained for CO (*Top*) and imaged for fluorescent signals (*Bottom*) in the same case as in (a). Yellow cells inside the *small and large white boxes* are shown at higher magnification in panels (c) and (d), respectively. *Dashed* contours delineate layer boundaries. Other conventions as in (a). Scale bars in (a-b): 500 μm. **(c-d)** V1→V2 starter cells (*arrowheads*) in L5 (c) and L6 (d), shown under GFP (*Top*) or mCherry (*Middle*) fluorescence, and merged (*Bottom*). Scale bars: 20 μm. **(e)** For each of the 3 cases, we show the percentage (left column) and the number (right bar graph) of V1→V2 starter cells across V1 layers. **(f)** Average percent of labeled starter cells across V1 layers for the population. Error bars: s.e.m. **(g)** Distribution of double-labeled V1 starter cell distances from the center of the nearest V1 injection site, plotted on the same axis as histograms (*Bottom*) and violin

plots (*Top*), for each of the 3 cases. The *black vertical line* in the violin plots is the median of the distribution.

Figure 3. V2 starter cells.
(a) Case MK405. Image of a V2 tissue sections stained for CO, revealing all layers. *Arrows* here and in (b) point to the V2 injection site, and *dashed contours* delineate the boundaries of L4. Scale bar: 500 µm (valid also for b). **(b)** Image of a V2 section immediately adjacent to the one in (a), imaged for mCherry and GFP and merged. Notice red fiber label in L4 and lower L3 representing m-Cherry labeled V1→V2 axon terminals. The region inside the *white box* is shown at higher magnification in (c). **(c)** A double-labeled pyramidal cell in V2 L3A shown under GFP (*Left*) or mCherry (*Middle*) fluorescence, and merged (*Right*). Scale bar: 20 µm. **(d)** Percent and number of V2 starter cells across layers for each of the two cases that had double-labeled cells in V2. **(e)** Distribution of double-labeled V2 cell distances from the center of the nearest V2 injection site for each case. Other conventions are as in **Fig. 2**.

Figure 4. V2 input cells.
(a-b) Case MK405. Images of two tangential sections through V2 L2/3-4 (a) and L2/3-6 (b) stained for CO (*Top*) after being imaged for mCherry and GFP fluorescence (*Middle*). The middle panels show the merged fluorescent channels. *Arrows*: V2 injection sites; white *arrowheads:* GFP-labeled input neurons; *yellow arrowhead:* a double-labeled starter cell in V2 L2/3. Red fibers are the terminals of V1→V2 neurons in L3-4. *Solid white contour:* V1/V2 border (V1 is below the border). Other conventions as in **Figs. 2-3.** *Bottom:* GFP-labeled V2 input cells in L3 (a) and L5 (b), shown under GFP (*Left*) or mCherry (*Middle*) fluorescence, and merged (*Right*). Scale bars in (a-b): 500 µm (*Top*), 100µm (*Bottom*). **(c)** Percent and number of V2 input cells across layers for each of the three cases. **(d)** Average percent of V2 input cells across V2 layers for the population. **(e)** Distribution of V2 input cell distances from the center of the V2 injection site. **(f)** Average ratio of V2 input cells in each layer to the total number of V1→V2 starter cells for the population. Error bars: s.e.m.

Figure 5. Case MK379: FB inputs from higher extrastriate cortex.
(a) Image of a sagittal section through extrastriate cortex encompassing the anterior bank of the lunate sulcus (*LS*), the prelunate gyrus and the banks of the superior temporal sulcus (*STS*), stained for myelin using the Gallyas method to reveal areal borders (*solid black lines*). *P:* posterior; *V:* ventral. **(b)** Higher magnification of the MT region inside the *black box* in (a) in an adjacent section imaged for GFP and mCherry fluorescence and merged. A single GFP-labeled pyramidal cell is visible in L5 (inside *white box*), and shown at higher magnification in (e). **(c)** Same as in (a) but for a different section. **(d)** Higher magnification of the V3d/V3A region inside the *white box* in (c) viewed under fluorescence. A single GFP-labeled cell is visible in L6 of dorsal V3 (V3d) (inside *white box*), and shown at higher magnification in (f). **(e-f)** GFP-labeled cells in MT L5 and V3d L6, respectively. Scale bars: 1 mm (a-c), 250 µm (b,d), 20 µm (e-f). **(g)** Number of GFP-labeled cells in higher extrastriate areas.

Figure 6. V1 input cells.
(a) Case MK405. Image of a single tangential section through V1 L2/3-4C stained for CO (*Left*) after being imaged for mCherry and GFP fluorescence (*Right*). The merged channel shows labeled

V1 input cells in L2/3, 4A, 4B and 4C (*green*) away from the injection sites (*arrows*). The region inside the *boxes* are shown at higher magnification in (b and c). Other conventions as in **Fig. 2**. Scale bar: 500µm. **(b-c**) GFP-labeled V1 input cells in L2/3 (b) and L4B (c), shown under GFP (*Left*) or mCherry (*Middle*) fluorescence, and merged (*Right*). Scale bars: 50µm. **(d)** Percent and number of V1 input cells across layers for each of the three cases. **(e)** Average percent of V1 input cells across V1 layers for the population. **(f)** Distribution of V1 input cell distances from the center of the nearest V1 injection site for each case. **(g)** Average percent of cortical inputs arising from V2 versus V1 for the population. Error bars: s.e.m.

Figure 7. Thalamic input cells.
(a) Case MK379. Image of a single parasagittal section through the LGN viewed under GFP fluorescence (*Left*), stained for fluorescent Nissl (*Middle Left*), immunostained for Calbindin-Alexa647 (*Middle Right*), and with all 3 channels merged (*Right*). The GFP-labeled cells inside the top and bottom *white boxes* are shown at higher magnification in (b) and (c), respectively. The parvocellular (*P3-6*) and magnocellular (*M1-2*) LGN layers are labeled. *A*: anterior; *s*: ventral. Scale bar: 250 µm). **(b-c**) GFP-labeled LGN input cells in the P3 (b) and M1 (c) layers shown in the same 3 channels as the top panels and with all channels merged (*Right*). *White arrowheads* point to the location of GFP-labeled neurons, *yellow arrowheads* point to calbindin-positive cells. The GFP-labeled cells are not calbindin-positive. Scale bars: 50 µm. **(d)** Image of a sagittal section through the LGN and pulvinar, with all 3 fluorescent channels (GFP, calbindin and Nissl) merged. The cells inside the *white box* are shown at higher magnification in (e). *PL*: lateral pulvinar; *PI*: inferior pulvinar; *LV*: lateral ventricle. Scale bar: 1 mm. **(e)** A GFP-labeled input cell (*white arrowhead*) in the PL imaged under the same 3 channels as for the LGN cells and with all channels merged (*Bottom Right*). *Yellow arrowhead* in each panel points to the location of a calbindin-positive cell (red). The GFP-labeled cell is not calbindin-positive. Scale bar: 50 µm. **(f)** Number of GFP-labeled cells in the thalamic nuclei. **(g)** Number of GFP-labeled cells in the LGN layers.

Figure 8. Summary circuit model.
Schematics of the FB circuit motifs discovered in this study. *Triangles*: pyramidal cell somata; *circles:* thalamic cell somata; *arrows*: axonal projections (thickness indicates projection magnitude). All axonal projections in this scheme are excitatory and terminate on excitatory cells. V2 FB neurons (*top blue cell*) make monosynaptic contacts with V1 neurons projecting to V2 (*green pyramidal cell*). The latter receive the majority of their long-range cortical inputs from other pyramidal neurons within V1 (*red cell*). V2 neurons in L5 sending FB to V1 and long-range connections within V2 (*bottom blue cell*) receive monosynaptic inputs from FB neurons in higher extrastriate areas (*blue cell*), as well as sparse inputs from the LGN and lateral pulvinar (*round green cells*). It is unclear whether the V2 L5 FB cells project to V1→V2 neurons or to other neurons within V1 (*?*).

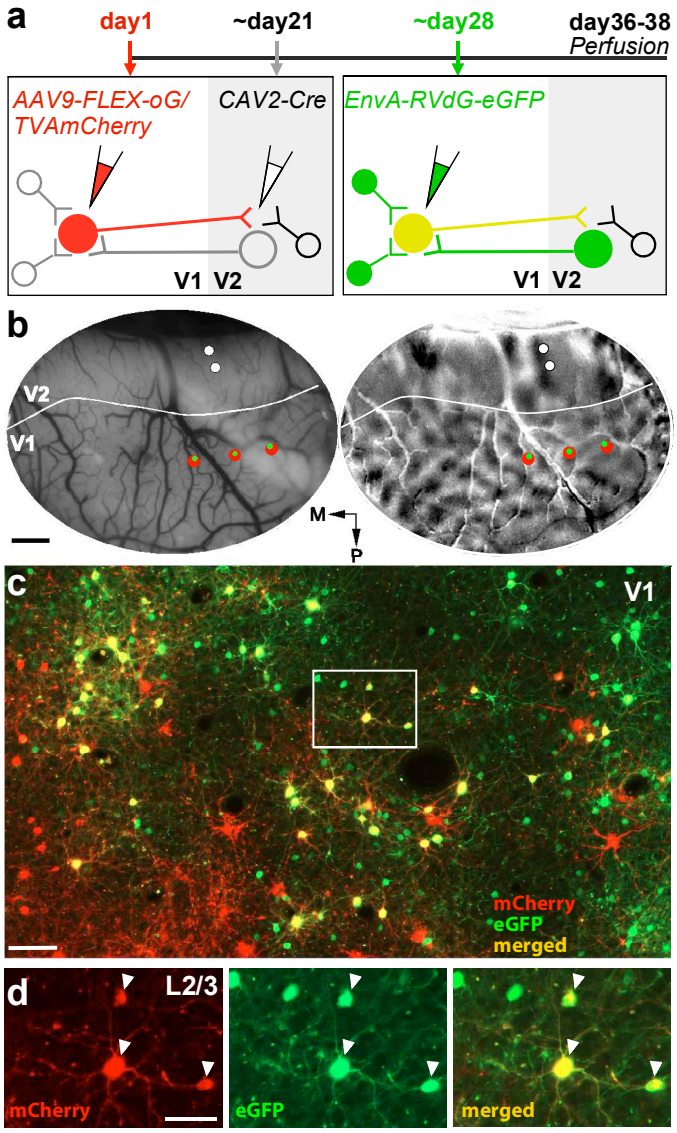
a
day1
~day21
~day28
day36-38
Perfusion
AAV9-FLEX-oG/
TVAmCherry
CAV2-Cre
EnvA-RVdG-eGFP
V1 V2
V1 V2
b
V2
V1
M
P
c
V1
mCherry
eGFP
merged
d
L2/3
mCherry
eGFP
merged

Figure 1

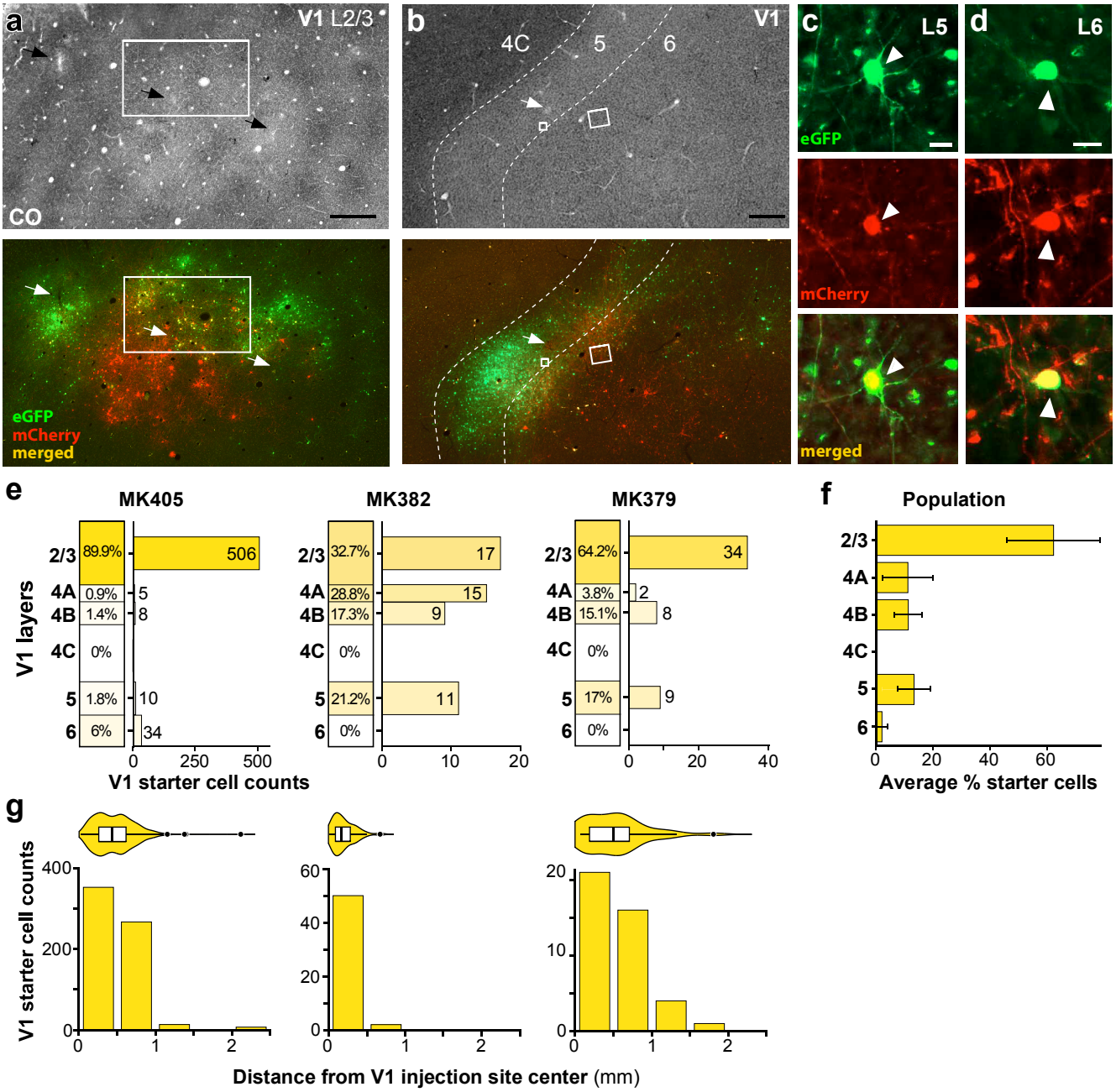
a
V1 L2/3
CO
b
V1
4C
5
6
c
L5
eGFP
d
L6
mCherry
merged
e
MK405
MK382
MK379
V1 layers
2/3
4A
4B
4C
5
6
89.9%
506
0.9%
5
1.4%
8
0%
1.8%
10
6%
34
32.7%
17
28.8%
15
17.3%
9
0%
21.2%
11
0%
64.2%
34
3.8%
2
15.1%
8
0%
17%
9
0%
V1 starter cell counts
f
Population
Average % starter cells
g
V1 starter cell counts
Distance from V1 injection site center (mm)

Figure 2

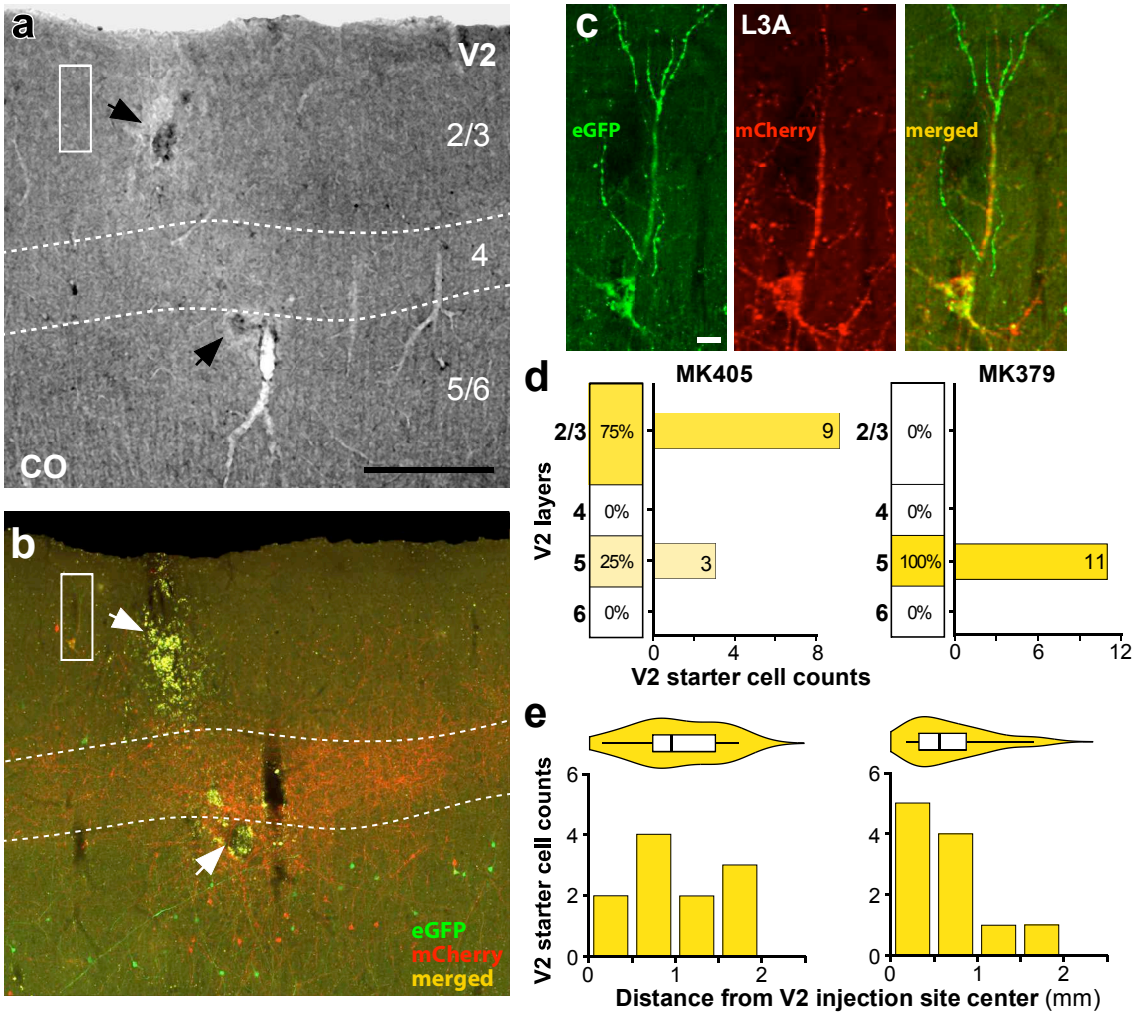
a
V2
2/3
4
5/6
CO
b
eGFP
mCherry
merged
c
L3A
eGFP
mCherry
merged
d
MK405
MK379
V2 layers
2/3
4
5
6
75%
0%
25%
0%
9
3
0%
0%
100%
0%
11
0
4
8
0
6
12
V2 starter cell counts
e
V2 starter cell counts
0
2
4
6
0
1
2
Distance from V2 injection site center (mm)

Figure 3

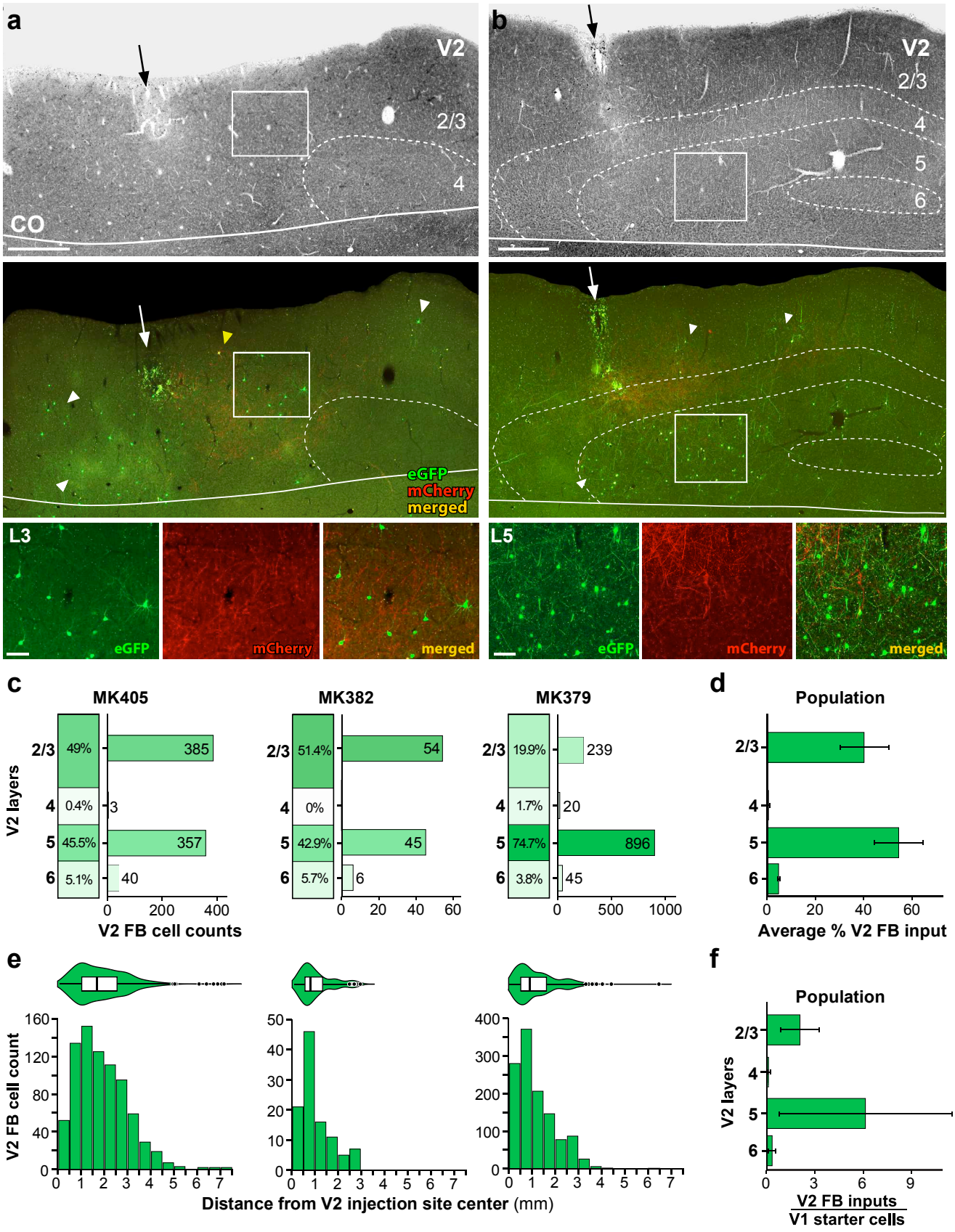
a
V2
2/3
4
CO
b
V2
2/3
4
5
6
eGFP
mCherry
merged
L3
eGFP
mCherry
merged
L5
eGFP
mCherry
merged
c
MK405
MK382
MK379
V2 layers
2/3
4
5
6
49%
385
0.4%
3
45.5%
357
5.1%
40
51.4%
54
0%
42.9%
45
5.7%
6
19.9%
239
1.7%
20
74.7%
896
3.8%
45
V2 FB cell counts
d
Population
Average % V2 FB input
e
V2 FB cell count
Distance from V2 injection site center (mm)
f
Population
V2 layers
V2 FB inputs
V1 starter cells

Figure 4

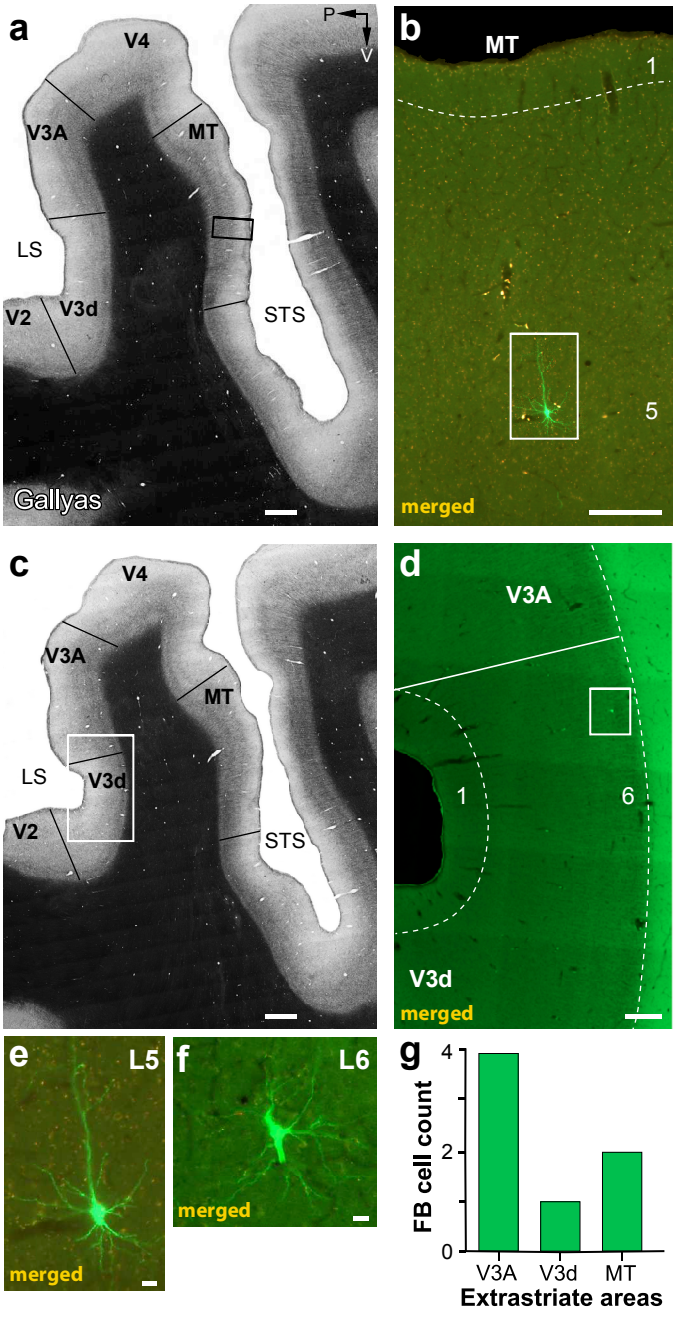
a
V4
P
V
V3A
MT
LS
V2
V3d
STS
Gallyas
b
MT
1
5
merged
c
V4
V3A
MT
LS
V3d
V2
STS
d
V3A
1
6
V3d
merged
e
L5
merged
f
L6
merged
g
FB cell count
4
2
0
V3A
V3d
MT
Extrastriate areas

Figure 5

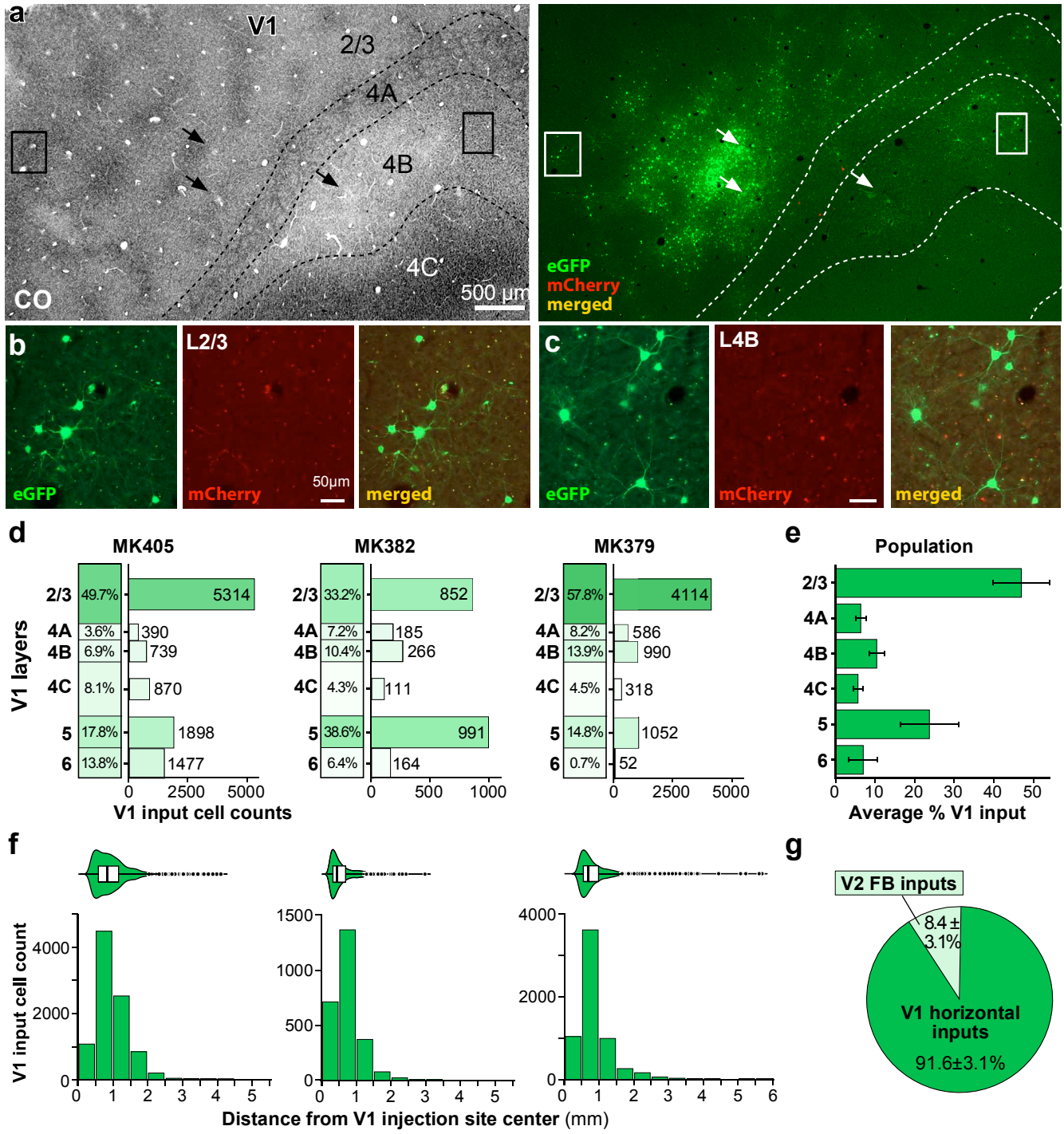
a
V1
2/3
4A
4B
4C'
CO
500 µm
eGFP
mCherry
merged
b
L2/3
eGFP
mCherry
50µm
merged
c
L4B
eGFP
mCherry
merged
d
MK405
MK382
MK379
V1 layers
2/3 49.7% 5314
4A 3.6% 390
4B 6.9% 739
4C 8.1% 870
5 17.8% 1898
6 13.8% 1477
2/3 33.2% 852
4A 7.2% 185
4B 10.4% 266
4C 4.3% 111
5 38.6% 991
6 6.4% 164
2/3 57.8% 4114
4A 8.2% 586
4B 13.9% 990
4C 4.5% 318
5 14.8% 1052
6 0.7% 52
V1 input cell counts
e
Population
Average % V1 input
f
V1 input cell count
Distance from V1 injection site center (mm)
g
V2 FB inputs
8.4 ± 3.1%
V1 horizontal inputs
91.6±3.1%

Figure 6

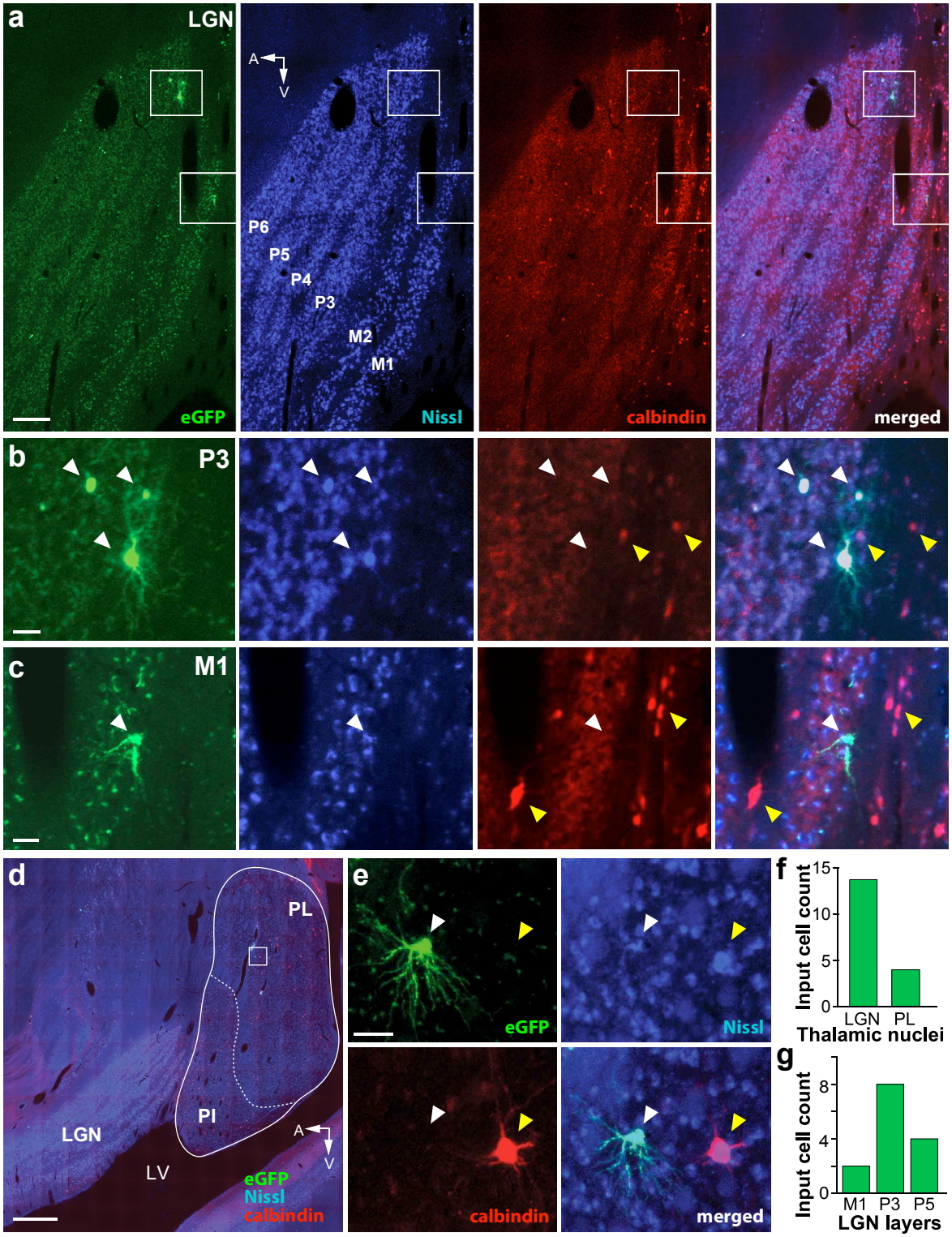
a
LGN
A
V
P6
P5
P4
P3
M2
M1
eGFP
Nissl
calbindin
merged
b
P3
c
M1
d
PL
PI
LGN
LV
A
V
eGFP
Nissl
calbindin
e
eGFP
Nissl
calbindin
merged
f
Input cell count
15
10
5
0
LGN
PL
Thalamic nuclei
g
Input cell count
8
4
0
M1
P3
P5
LGN layers

Figure 7

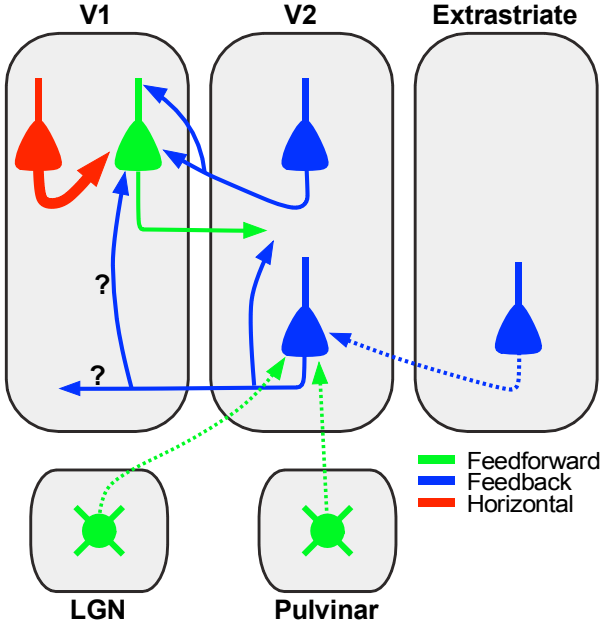
V1
V2
Extrastriate
?
?
Feedforward
Feedback
Horizontal
LGN
Pulvinar

Figure 8

Figures

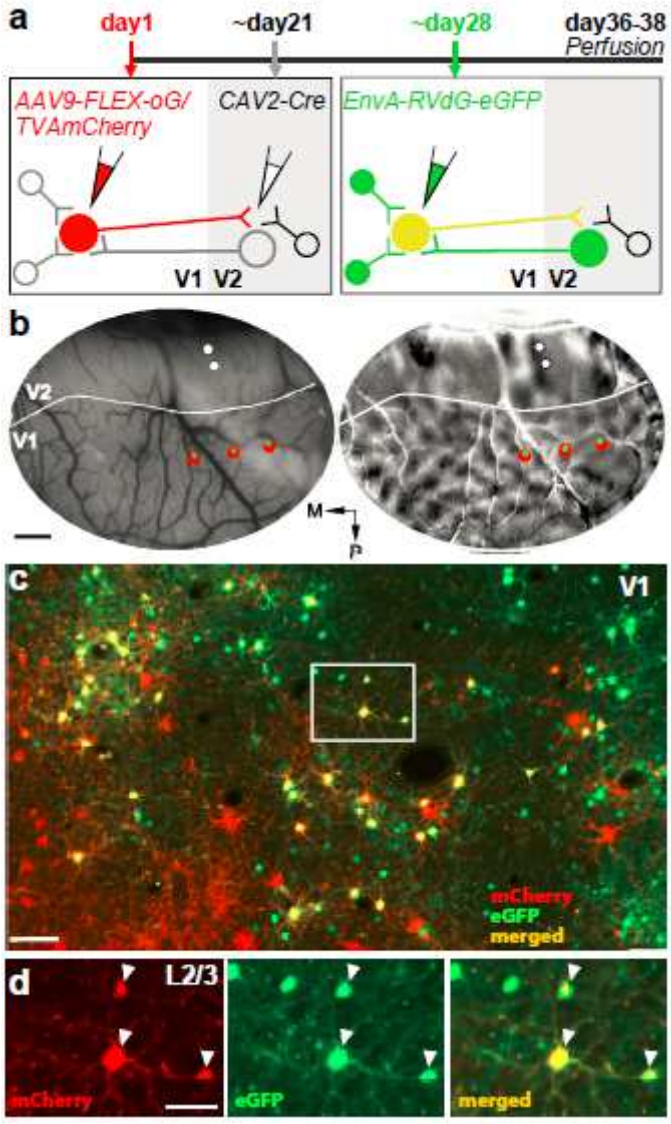

Figure 1

Monosynaptic input tracing in macaque visual cortex: experimental procedure. (a) Viral injection timeline and experimental design. Left: V1àV2 neurons express mCherry (red cells), TVA and oG, after double infection with AAV9-vectors (injected in V1) and CAV2-Cre (injected in V2). Right: After additional infection with EnvA-RVdG-eGFP (injected at the same V1 sites as AAV9), V1àV2 neurons previously infected with AAV9 additionally express eGFP, becoming double-labeled (yellow starter cells). After trans-synaptic RVdG-eGFP infection, V1 and V2 cells presynaptic to the V1 starter cells express eGFP (green cells). Cells that are not coinfected with both CAV2 and AAV9 remain unlabeled. (b) In vivo OI of V1 and V2 in one example case (MK405). Left: Image of the cortical surface vasculature encompassing V1 and V2. Solid white contour: V1-V2 border. The surface vasculature is used as reference to target viral injections to matching retinotopic positions in V1 and V2. Red, green and white spots: locations of AAV9, RVdG and CAV2 injections, respectively. Right: Difference orientation map of V1 and V2 obtained by subtracting

responses to achromatic luminance gratings of one orientation from gratings of the orthogonal orientation. V2 can be distinguished from V1 due to its “stripy” pattern and larger orientation domains. M: Medial; P: posterior. Scale bar: 1 mm. (c) Case MK405. Image of the viral injection sites through V1 layers 2/3 taken under mCherry and GFP fluorescence, and then merged. Red cells: V1àV2 neurons co-infected with CAV2 and AAV9 vectors, but not with RVdG vector. Yellow cells: starter V1àV2 cells double-labeled due to triple infection with all 3 viral vectors. Green cells: cells sending monosynaptic input to the starter V1àV2 cells (but some local V1 green label is due to TVA “leak” – see Results and Extended Data Fig. 1). Scale bar: 100 µm. Cells in the boxed region are shown at higher magnification in (d) (d) Higher magnification of 3 starter V1àV2 cells (arrowheads) shown under mCherry (Left) or GFP fluorescence (Middle), and merged (Right). Scale bar: 50 µm.

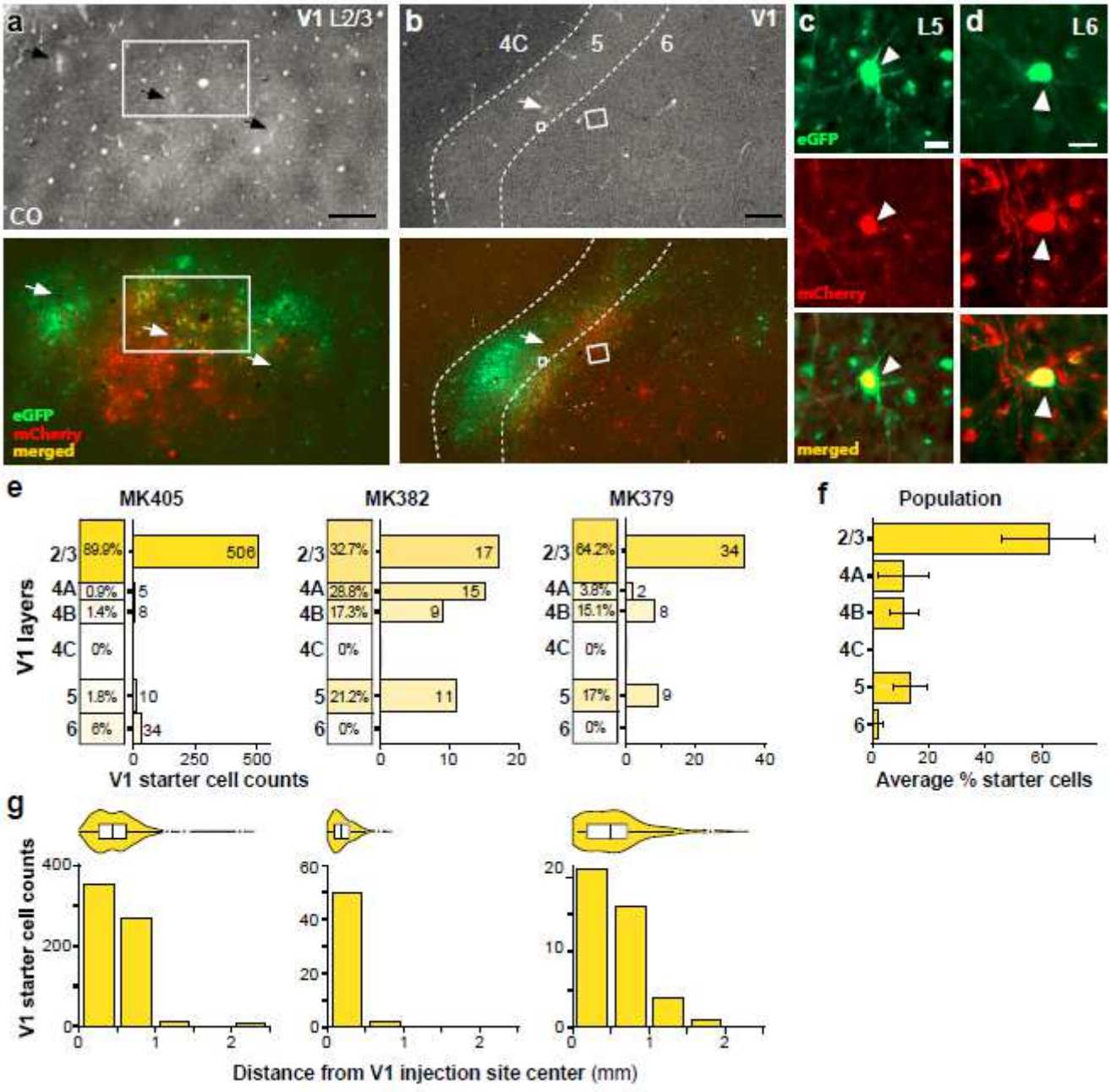

Figure 2

V1->V2 starter cells. (a) Case MK405. Image of a single tangential section through V1 L2/3 stained for CO (Top) after being imaged for mCherry and GFP fluorescence (Bottom). The merged channel shows starter V1->V2cells (yellow). Arrows point to the V1 injection sites in both sections, which are recognizable as discoloration in CO staining. The region inside the white box is shown at higher magnification in panel (c). (b) Image of a single tangential section through V1 L4C-6 stained for CO (Top) and imaged for fluorescent signals (Bottom) in the same case as in (a). Yellow cells inside the small and large white boxes are shown at higher magnification in panels (c) and (d), respectively. Dashed contours delineate layer boundaries. Other conventions as in (a). Scale bars in (a-b): 500 µm. (c-d) V1->V2 starter cells (arrowheads) in L5 (c) and L6 (d), shown under GFP (Top) or mCherry (Middle) fluorescence, and merged (Bottom). Scale bars: 20 µm. (e) For each of the 3 cases, we show the percentage (left column) and the number (right bar graph) of V1àV2 starter cells across V1 layers. (f) Average percent of labeled starter cells across V1 layers for the population. Error bars: s.e.m. (g) Distribution of double-labeled V1 starter cell distances from the center of the nearest V1 injection site, plotted on the same axis as histograms (Bottom) and violin plots (Top), for each of the 3 cases. The black vertical line in the violin plots is the median of the distribution.

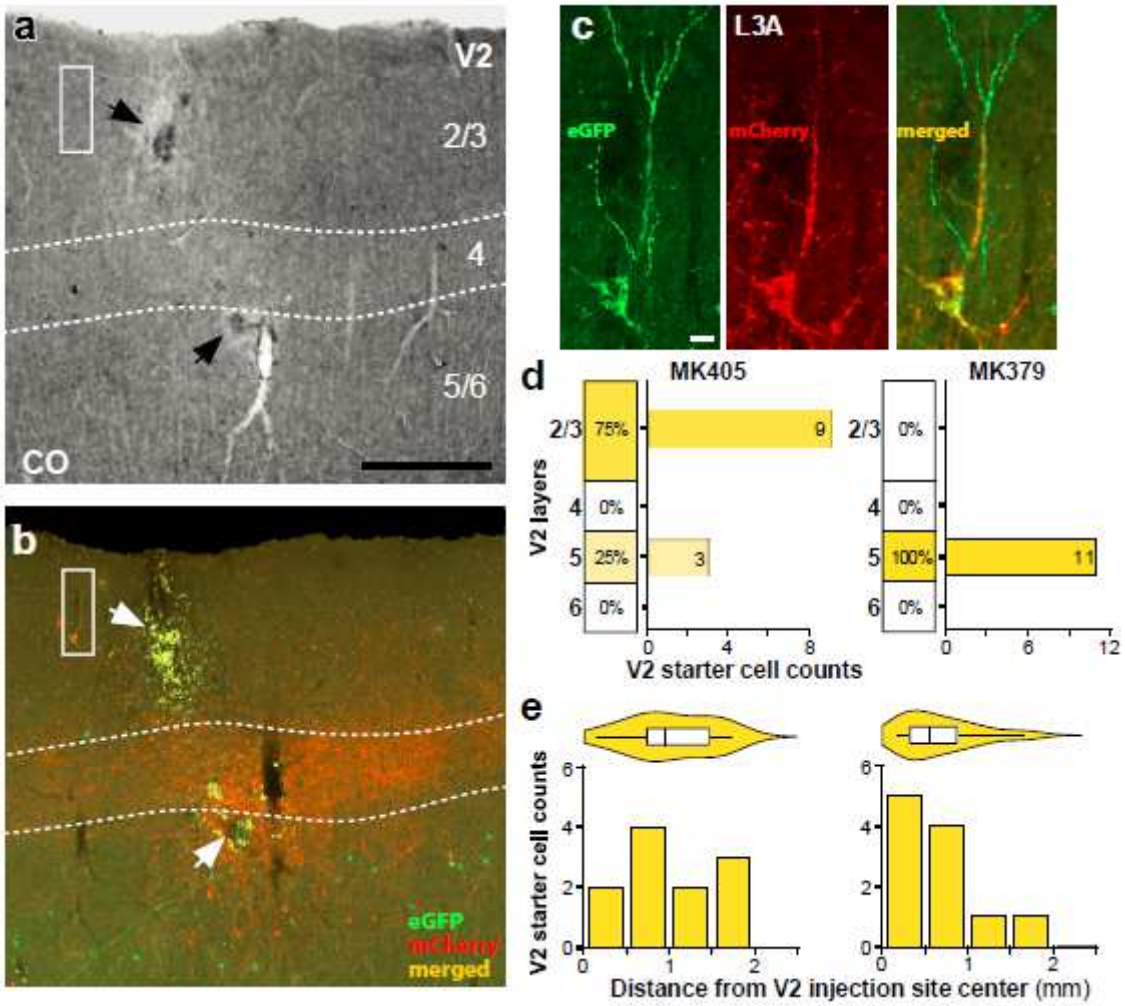

Figure 3

V2 starter cells. (a) Case MK405. Image of a V2 tissue sections stained for CO, revealing all layers. Arrows here and in (b) point to the V2 injection site, and dashed contours delineate the boundaries of L4. Scale bar: 500 μm (valid also for b). (b) Image of a V2 section immediately adjacent to the one in (a), imaged for mCherry and GFP and merged. Notice red fiber label in L4 and lower L3 representing m-Cherry labeled V1àV2 axon terminals. The region inside the white box is shown at higher magnification in (c). (c) A double-labeled pyramidal cell in V2 L3A shown under GFP (Left) or mCherry (Middle) fluorescence, and merged (Right). Scale bar: 20 μm. (d) Percent and number of V2 starter cells across layers for each of the two cases that had double-labeled cells in V2. (e) Distribution of double-labeled V2 cell distances from the center of the nearest V2 injection site for each case. Other conventions are as in Fig. 2.

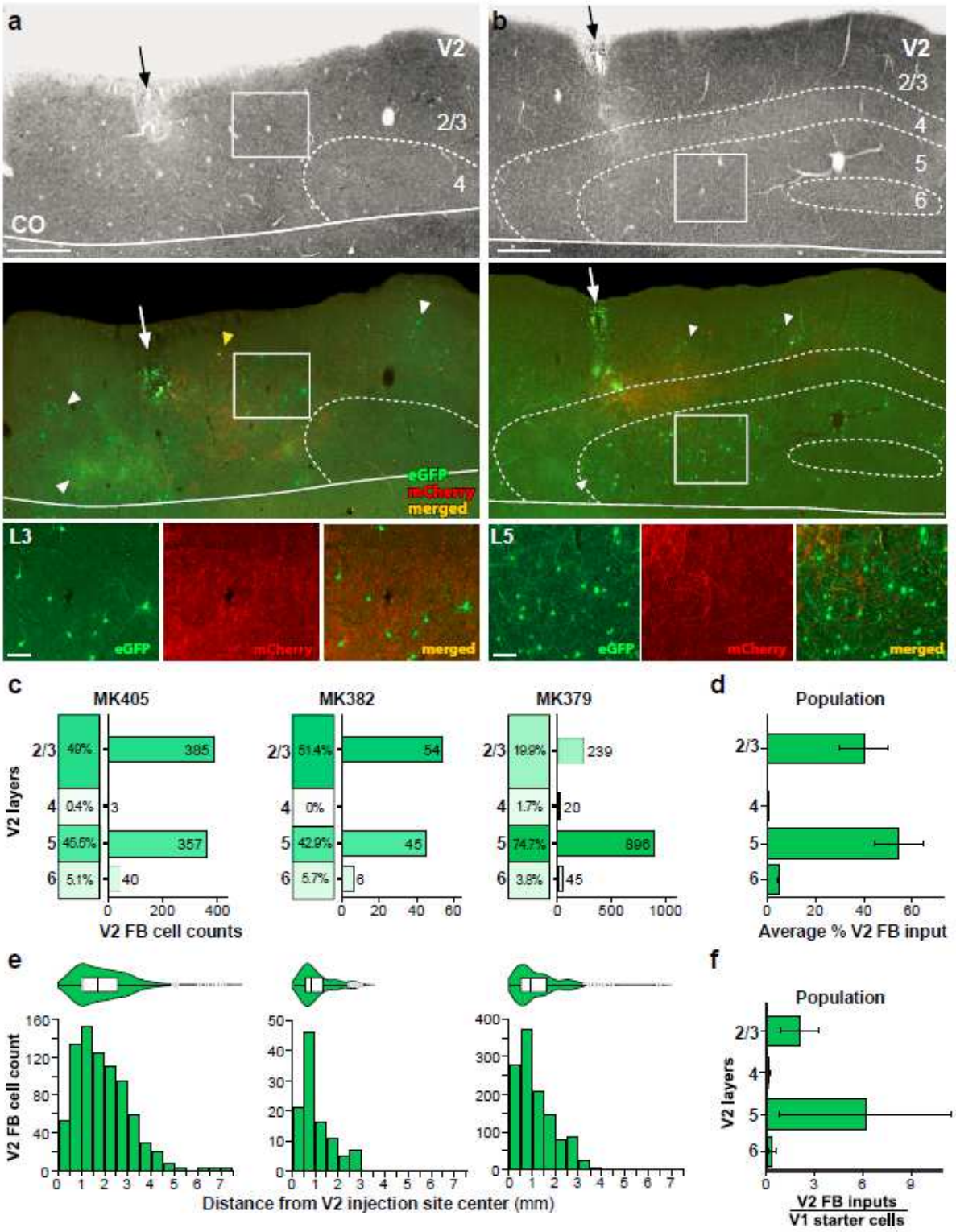

Figure 4

V2 input cells. (a-b) Case MK405. Images of two tangential sections through V2 L2/3-4 (a) and L2/3-6 (b) stained for CO (Top) after being imaged for mCherry and GFP fluorescence (Middle). The middle panels show the merged fluorescent channels. Arrows: V2 injection sites; white arrowheads: GFP-labeled input neurons; yellow arrowhead: a double-labeled starter cell in V2 L2/3. Red fibers are the terminals of V1àV2 neurons in L3-4. Solid white contour: V1/V2 border (V1 is below the border). Other conventions as in Figs.

2-3. Bottom: GFP-labeled V2 input cells in L3 (a) and L5 (b), shown under GFP (Left) or mCherry (Middle) fluorescence, and merged (Right). Scale bars in (a-b): 500 µm (Top), 100µm (Bottom). (c) Percent and number of V2 input cells across layers for each of the three cases. (d) Average percent of V2 input cells across V2 layers for the population. (e) Distribution of V2 input cell distances from the center of the V2 injection site. (f) Average ratio of V2 input cells in each layer to the total number of V1àV2 starter cells for the population. Error bars: s.e.m.

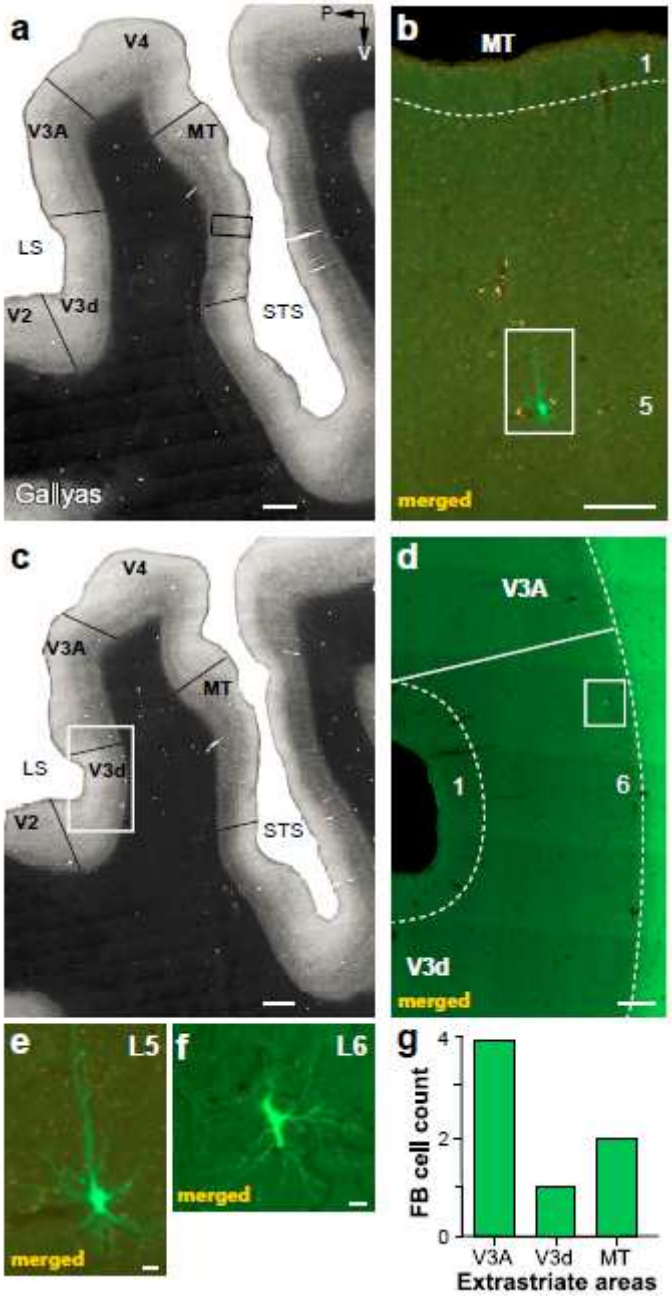

Figure 5

Case MK379: FB inputs from higher extrastriate cortex. (a) Image of a sagittal section through extrastriate cortex encompassing the anterior bank of the lunate sulcus (LS), the prelunate gyrus and the banks of the superior temporal sulcus (STS), stained for myelin using the Gallyas method to reveal areal

borders (solid black lines). P: posterior; V: ventral. (b) Higher magnification of the MT region inside the black box in (a) in an adjacent section imaged for GFP and mCherry fluorescence and merged. A single GFP-labeled pyramidal cell is visible in L5 (inside white box), and shown at higher magnification in (e). (c) Same as in (a) but for a different section. (d) Higher magnification of the V3d/V3A region inside the white box in (c) viewed under fluorescence. A single GFP-labeled cell is visible in L6 of dorsal V3 (V3d) (inside white box), and shown at higher magnification in (f). (e-f) GFP-labeled cells in MT L5 and V3d L6, respectively. Scale bars: 1 mm (a-c), 250 µm (b,d), 20 µm (e-f). (g) Number of GFP-labeled cells in higher extrastriate areas.

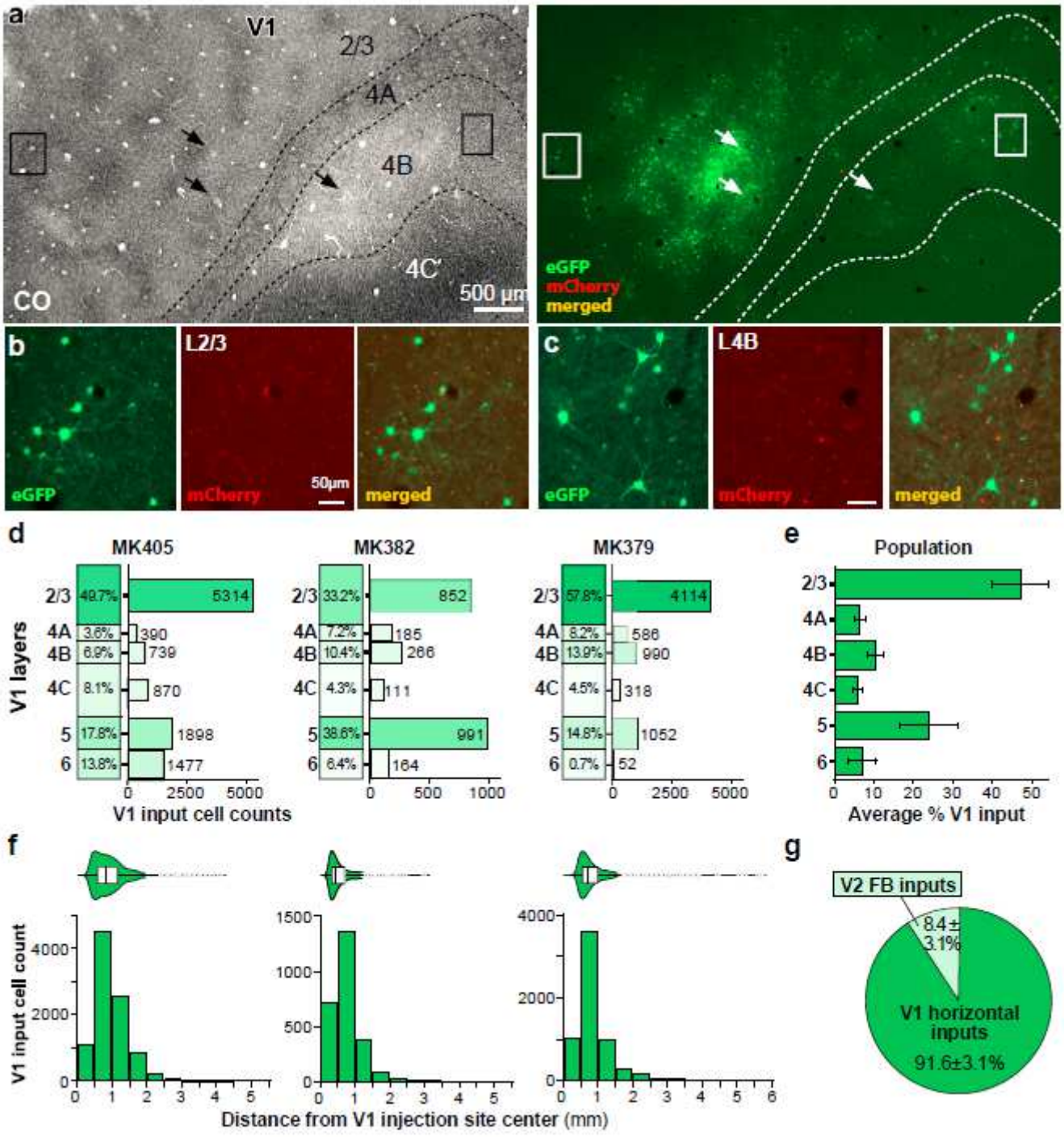

Figure 6

V1 input cells. (a) Case MK405. Image of a single tangential section through V1 L2/3-4C stained for CO (Left) after being imaged for mCherry and GFP fluorescence (Right). The merged channel shows labeled V1 input cells in L2/3, 4A, 4B and 4C (green) away from the injection sites (arrows). The region inside the boxes are shown at higher magnification in (b and c). Other conventions as in Fig. 2. Scale bar: 500μm. (b-c) GFP-labeled V1 input cells in L2/3 (b) and L4B (c), shown under GFP (Left) or mCherry (Middle) fluorescence, and merged (Right). Scale bars: 50μm. (d) Percent and number of V1 input cells across layers for each of the three cases. (e) Average percent of V1 input cells across V1 layers for the population. (f) Distribution of V1 input cell distances from the center of the nearest V1 injection site for each case. (g) Average percent of cortical inputs arising from V2 versus V1 for the population. Error bars: s.e.m.

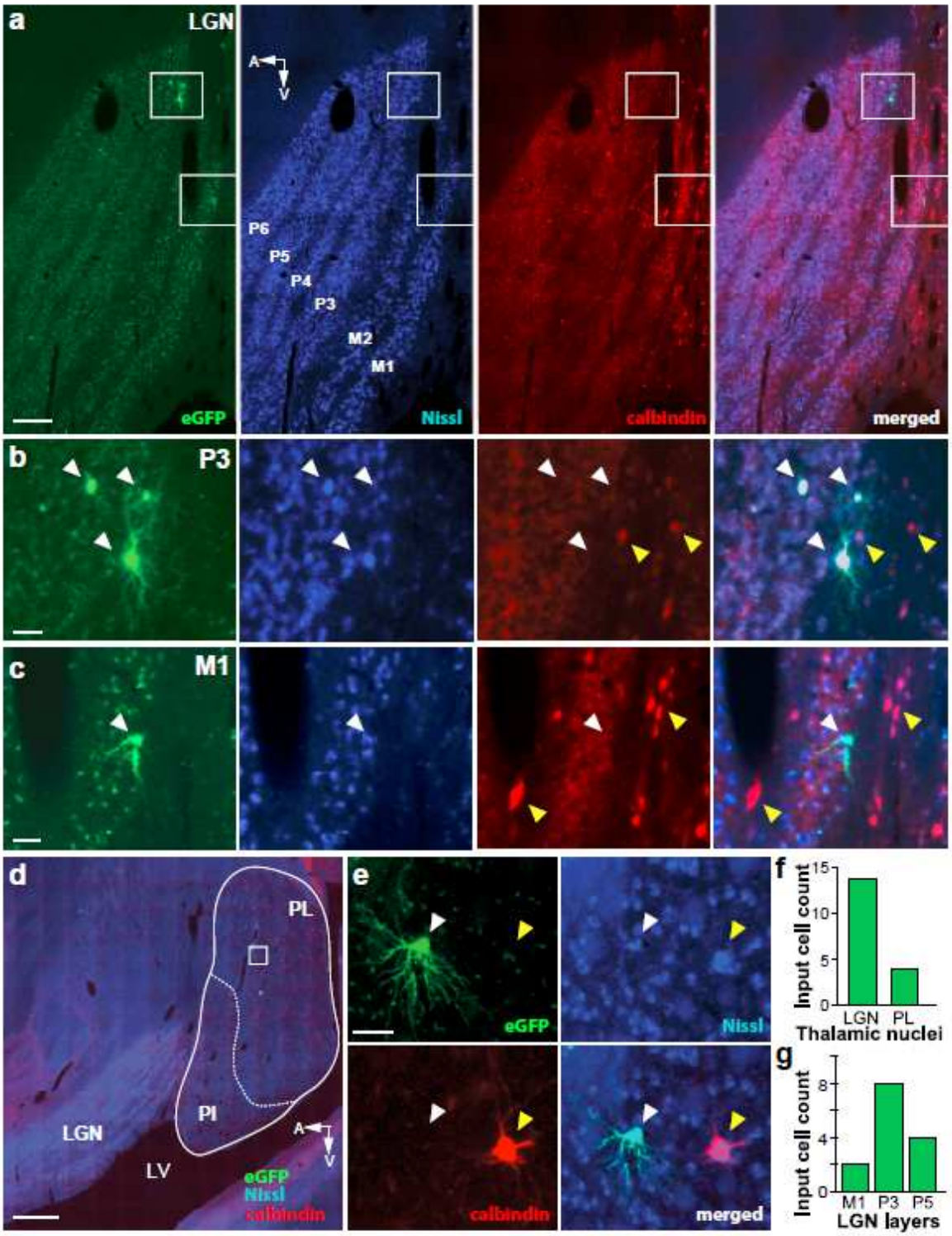

Figure 7

Thalamic input cells. (a) Case MK379. Image of a single parasagittal section through the LGN viewed under GFP fluorescence (Left), stained for fluorescent Nissl (Middle Left), immunostained for Calbindin-Alexa647 (Middle Right), and with all 3 channels merged (Right). The GFP-labeled cells inside the top and bottom white boxes are shown at higher magnification in (b) and (c), respectively. The parvocellular (P3-6) and magnocellular (M1-2) LGN layers are labeled. A: anterior; s: ventral. Scale bar: 250 μm). (b-c) GFP-

labeled LGN input cells in the P3 (b) and M1 (c) layers shown in the same 3 channels as the top panels and with all channels merged (Right). White arrowheads point to the location of GFP-labeled neurons, yellow arrowheads point to calbindin-positive cells. The GFP-labeled cells are not calbindin-positive. Scale bars: 50 µm. (d) Image of a sagittal section through the LGN and pulvinar, with all 3 fluorescent channels (GFP, calbindin and Nissl) merged. The cells inside the white box are shown at higher magnification in (e). PL: lateral pulvinar; PI: inferior pulvinar; LV: lateral ventricle. Scale bar: 1 mm. (e) A GFP-labeled input cell (white arrowhead) in the PL imaged under the same 3 channels as for the LGN cells and with all channels merged (Bottom Right). Yellow arrowhead in each panel points to the location of a calbindinpositive cell (red). The GFP-labeled cell is not calbindin-positive. Scale bar: 50 µm. (f) Number of GFP-labeled cells in the thalamic nuclei. (g) Number of GFP-labeled cells in the LGN layers.

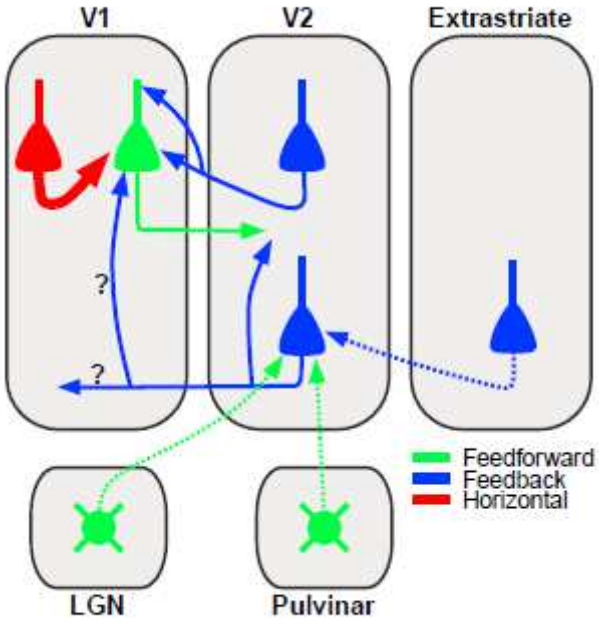

Figure 8

Summary circuit model. Schematics of the FB circuit motifs discovered in this study. Triangles: pyramidal cell somata; circles: thalamic cell somata; arrows: axonal projections (thickness indicates projection magnitude). All axonal projections in this scheme are excitatory and terminate on excitatory cells. V2 FB neurons (top blue cell) make monosynaptic contacts with V1 neurons projecting to V2 (green pyramidal cell). The latter receive the majority of their long-range cortical inputs from other pyramidal neurons within V1 (red cell). V2 neurons in L5 sending FB to V1 and long-range connections within V2 (bottom blue cell) receive monosynaptic inputs from FB neurons in higher extrastriate areas (blue cell), as well as sparse inputs from the LGN and lateral pulvinar (round green cells). It is unclear whether the V2 L5 FB cells project to V1àV2 neurons or to other neurons within V1 (?).

Supplementary Files

This is a list of supplementary files associated with this preprint. Click to download.

- ExtendedDataFig1.pdf
- SupplementaryTable1.pdf